

BLUE PRI A4 .5secs 13 JUL 84 YAU0018

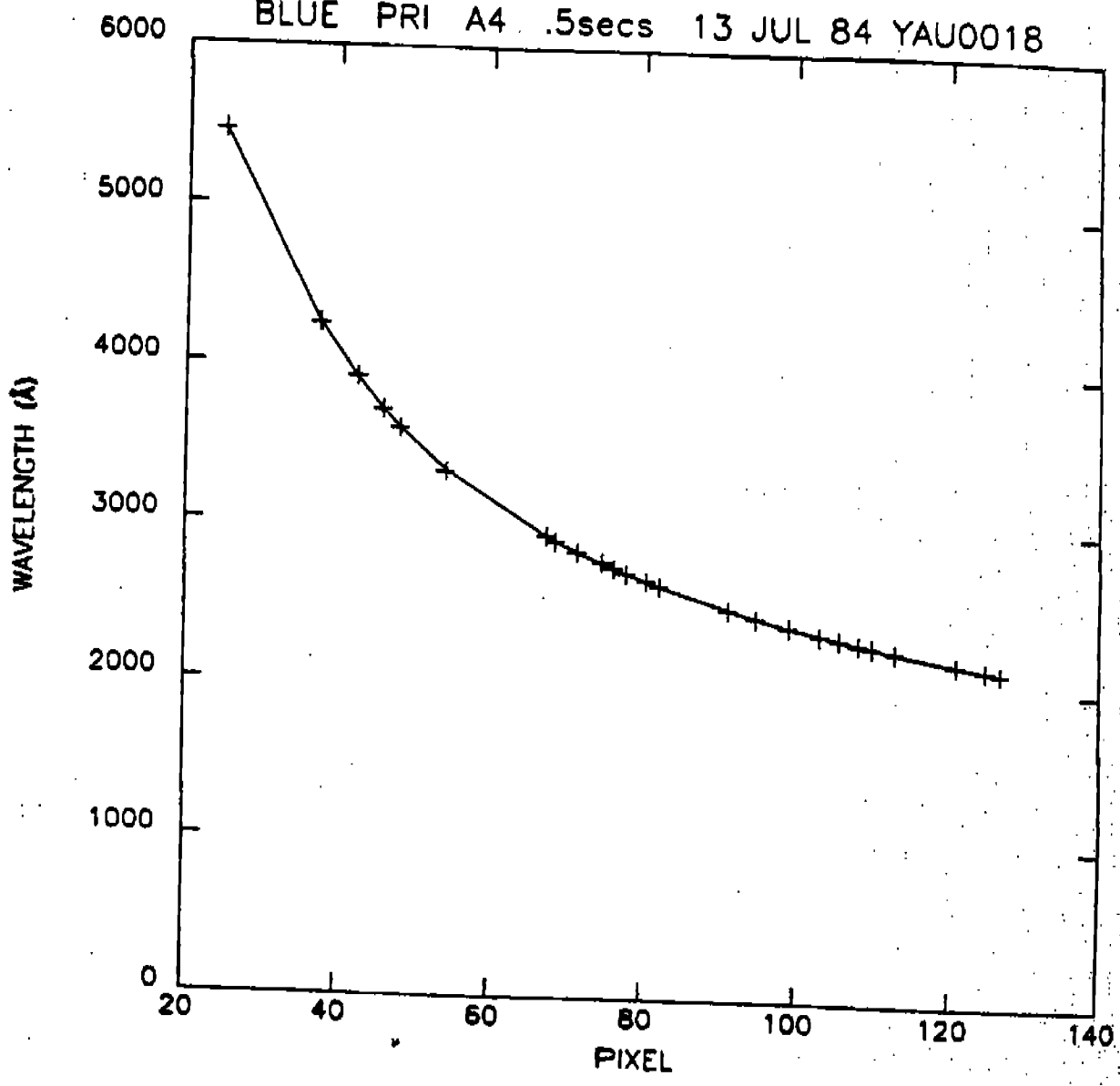


Figure 5.1-4. Wavelength as a function of pixel number for the prism, blue Digicon. The points are the measured pixel values and the curve is the nonlinear least squares fit to the points.

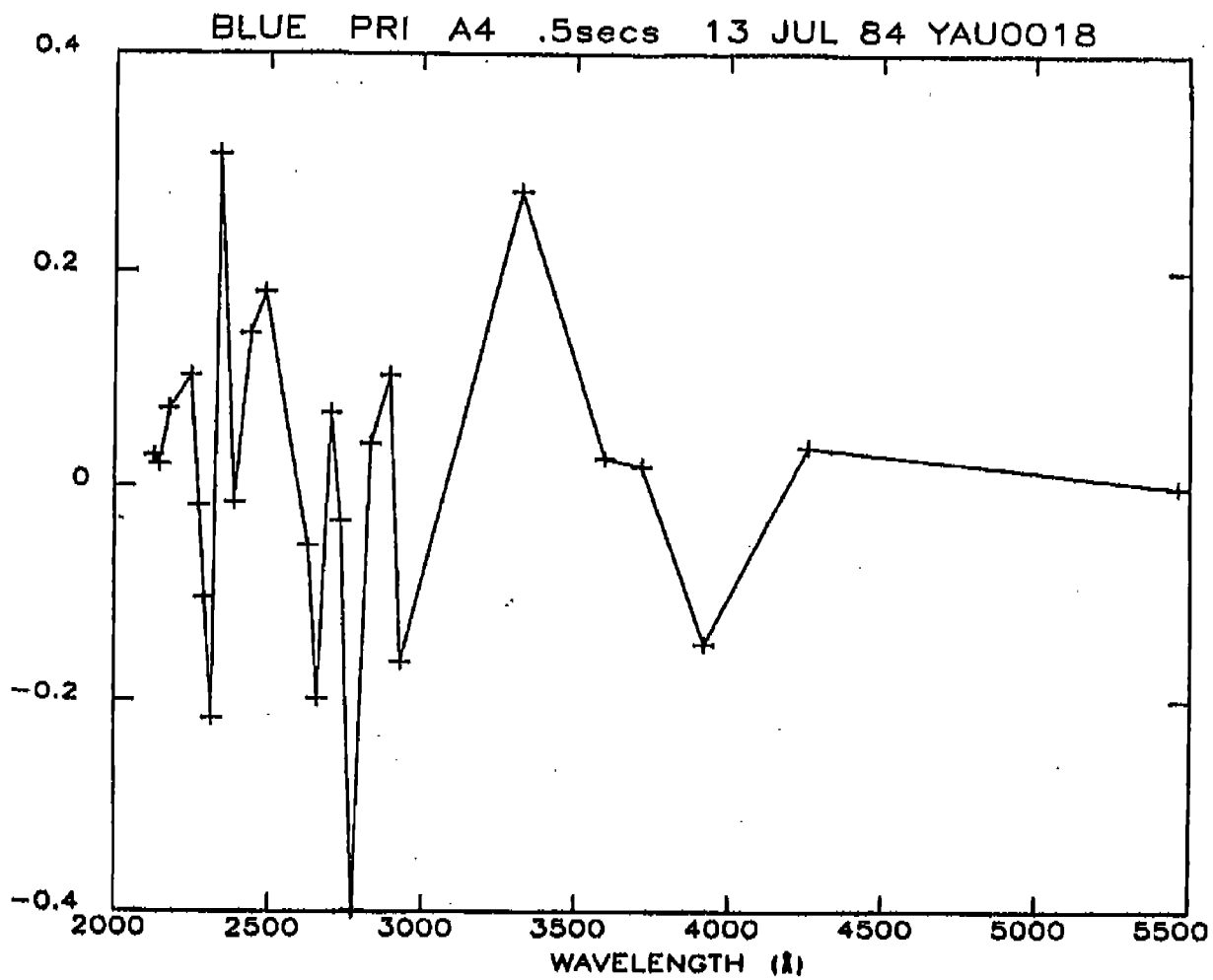


Figure 5.1-5. Plot of residuals from the fourth order expansion in $1/x$ vs. wavelength for the prism, blue detector.

blue side of the July 19 vacuum data vs. the residuals of the July 13 vacuum data shows a very strong correlation ($R = 0.916$, see Figure 5.1-6). Since this systematic error is present in four different blue spectra taken with two different gratings and at two different FOS operating temperatures, non-uniform spacing of the diode elements may be the source of the systematic errors at the few micron level.

Changes in the dispersion relations due to the use of all apertures other than the A4 lower will be deferred to Section 5.3.

5.2 Internal to External Offset

Any systematic wavelength shifts between internal and external sources were found to be unmeasurably small at less than 0.05 of a diode (or 2.5 microns).

5.3 Spectral Resolution: Line Widths (FWHM) as a Function of Aperture Size

When observing extended sources such as galaxies and nebulae which fill the FOS entrance aperture, the line profile will be a function of the aperture size. We have characterized the line widths for the ten entrance apertures on the red and the blue sides by measuring the FWHM of emission lines in spectra of an external calibration source taken during the last FOS thermal-vacuum calibration at Martin Marietta.

The FWHM's are approximately equal to the aperture size used in the observation. The widths do not appear to vary when different gratings are used, and the asymmetry for lines on the

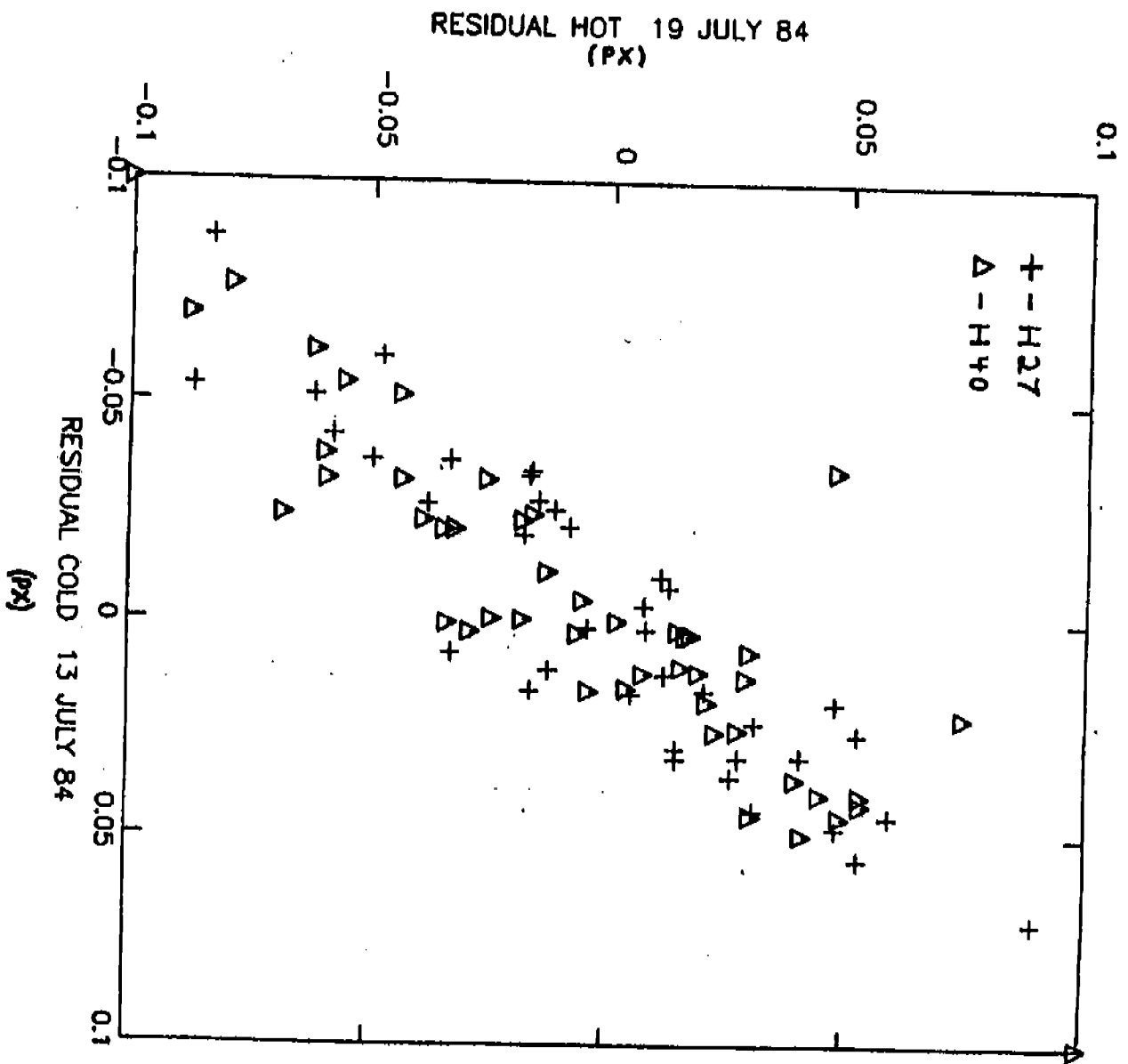


Figure 5.1-6. Scatter diagram of the residuals for the two independent vacuum data sets, blue detector. The cubic residuals (in pixels) from gratings H27 and H40 from the July 19 data are plotted against the cubic residuals from the July 13 data. Note the very strong correlation ($R = .915$).

edge of the diode array, as shown by a ray trace, appear negligible. For the smallest aperture, 80% of the light in the line falls within a width of one diode.

In general, the FWHM of emission lines for all apertures are approximately equal to the aperture size, for both the red and the blue tube. There are, however, several exceptions to this rule.

First, when an aperture is smaller than a diode, the FWHM is about the width of a diode, or 0.36λ . This holds for the smallest circular and square apertures, as can be seen in Table 5.3-1. Second, circular apertures have smaller FWHM than their square counterparts because of the relative areas. This can be seen by comparing the circular and square apertures of comparable size. Finally, the FWHM of lines taken with the largest aperture are smaller than the aperture size of 2.0λ . Instead of being flat topped, these lines are sloping, which implies that the illumination was not evenly distributed over the entrance aperture. This is the most likely cause of the relatively small FWHM for the 2.0λ aperture.

The widths of the emission lines do not appear to depend on the grating used. For the 0.25λ aperture with the blue tube, FWHM has been measured for several gratings (H13, H19, H40, H57, L15, and L65) and the prism. Two of these cases (L15 and the prism) have larger measured FWHM than expected from the 0.25λ aperture size. In each case, however, there are practically no well separated lines in the spectrum, so the larger FWHM are very likely due to the mixing of lines.

TABLE 5.3-1

FOS LINE WIDTHS (FWHM) AS A FUNCTION OF APERTURE SIZE*

<u>Designation</u>	<u>Size (")</u>	<u>H13 (Blue)</u>	<u>H87 (Red)</u>
0.30 SNG	0.3 (circular)	1.00 ± .01	0.95 ± .02
0.50 SNG	0.5 (circular)	1.27 ± .04	1.20 ± .01
1.00 SNG	1.0 (circular)	2.29 ± .02	2.23 ± .01
0.10 PAIR	0.10 (square)	0.97 ± .03	0.92 ± .02
0.25 PAIR	0.25 (square)	0.98 ± .01	0.96 ± .01
0.50 PAIR	0.50 (square)	1.30 ± .04	1.34 ± .02
1.00 PAIR	1.00 (square)	2.65 ± .02	2.71 ± .02
0.25 x 2.0	0.25 x 2.0 (slit)	0.99 ± .01	0.96 ± .01
0.70 x 2.0-BAR	0.70 x 2.0	1.83 ± .02	1.90 ± .01
2.0-BAR	2.0	5.28 ± .07	5.43 ± .04

*The FWHM are given in units of diodes

A ray trace of FOS has shown that a certain amount of asymmetry can be expected in line profiles for lines near the edge of the diode array (see ST End to End Optical Performance Analysis, ST/SE-24, Section F, page 7-3). On close inspection of well separated lines near the diode array edge, it appears that this asymmetry may give a small contribution to the broad, low level wings, but has a negligible affect on the FWHM.

The best present estimate of the percentage of light from the 0.1μ aperture that falls into one diode is 90%.

In order to analytically characterize the extended wings of the FOS line profiles, we have fit a pseudo Voight function to the Hg 2537 Å line profile (Blue side, aperture A4, grating H27) given by Sirk and Bohlin (1988; plot YAZ0322). The pseudo Voight function is given by Equations (5.3-1 and 5.3-2).

$$V(x, \gamma, w) = y_0 \left\{ \left[1 - \frac{\gamma}{w} \right] \exp \left[-\ln 2 \left(\frac{x - x_0}{w} \right)^2 \right] + \left[\frac{\gamma}{w} \right] \left[\frac{1}{1 + \left(\frac{x - x_0}{w} \right)^2} \right] \right\} \quad (5.3-1)$$

$$w = \frac{\gamma}{2} + \left(\frac{\gamma^2}{4} + 2 (\ln 2) \sigma^2 \right)^{\frac{1}{2}} \quad (5.3-2)$$

The quantity y_0 is the amplitude of the function (height of the line), γ is a parameter which characterizes the Lorentzian wings, σ is a parameter which characterizes the Gaussian core, and $x - x_0$ is the distance from the line center in diodes. In the limit that γ goes to zero, the function becomes a pure Gaussian as given by Equation 5.3-3.

$$G(x, \sigma) = y_0 \exp \left(\frac{-(x - x_0)^2}{2\sigma^2} \right) \quad (5.3-3)$$

The parameters of a good fit to the Hg 2537 Å line are $\sigma = 0.30$ and $\gamma = 0.07$. These parameters give values which are within 25% of the observed line profile out to 20 diodes from the line center. The Hg 2537 Å and Hg 5460 Å line profiles are very similar to one another, and the profiles of the same comparison line on the red and blue sides are quite similar. Consequently, the pseudo Voigt function with the above parameters can be used as a first approximation for the (small aperture) line profile everywhere.

6.0 PHOTOMETRIC CALIBRATION

6.1 Flat Field Measurements

The FOS photocathodes have a granularity of less than one percent. Nine blemishes, with sensitivity variations greater than 5 percent, were found on the red tube in regions illuminated by aperture A3. The spatial extent of the blemishes in the direction of the diode array range from 50 to 250 microns. Following the decision on whether or not to swap the red Digicon, a more complete analysis of the data for all apertures will be produced.

Data analyzed in this report were obtained in air in August, 1984 using a tungsten continuum lamp as the calibration source. The FOS was used in the recommended substepping mode, where the data were quarter stepped (XSTEPS = 4) and multiplexing over 5 diodes (OVRSON = 5) used to reduce variations due to the sensitivities of the diodes. Each observation contained four independent sampling of the same spectra (SLICES = 4). The data were analyzed for the upper and lower C1 (1.0 arcsec) apertures, except for the prism on the red side where the A3 (0.25 arcsec) aperture was used.

All data were corrected for diode nonlinearities (paired pulse correction). The counts in data points scanned by dead diodes were adjusted accordingly (i.e., multiplication of the data value by 5/(number of good diodes sampling the data). The plots in Figures 6.1-1 through 6.1-8 show the corrected counts for each slice. The upper three slices are offset incrementally

FIGURE 6.1-1

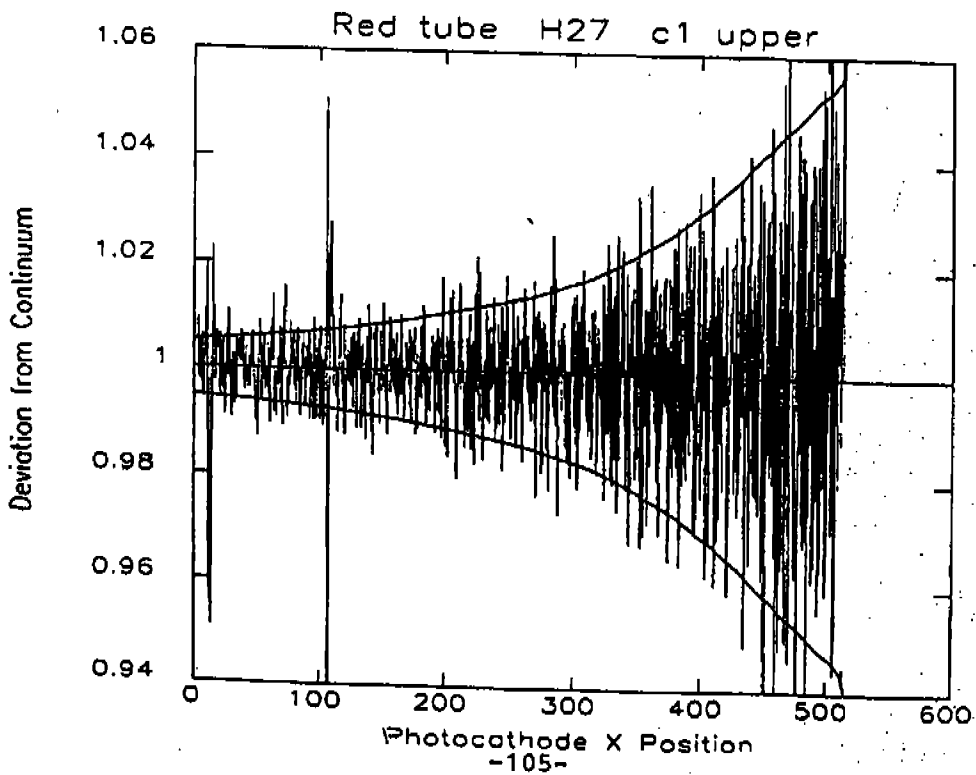
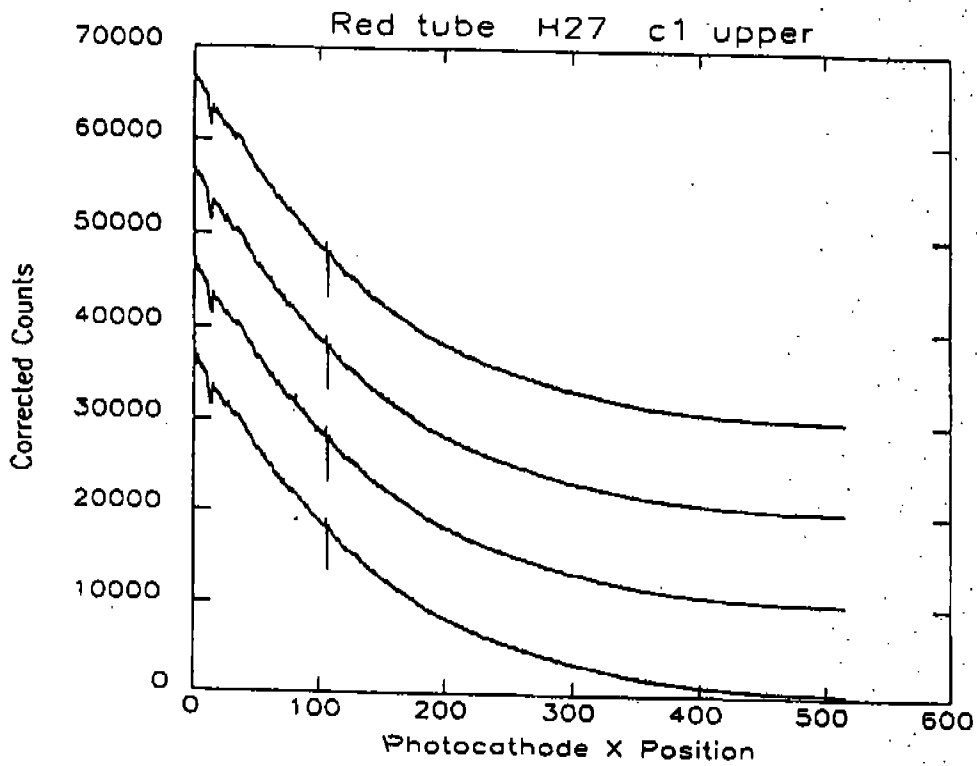


FIGURE 6.1-2

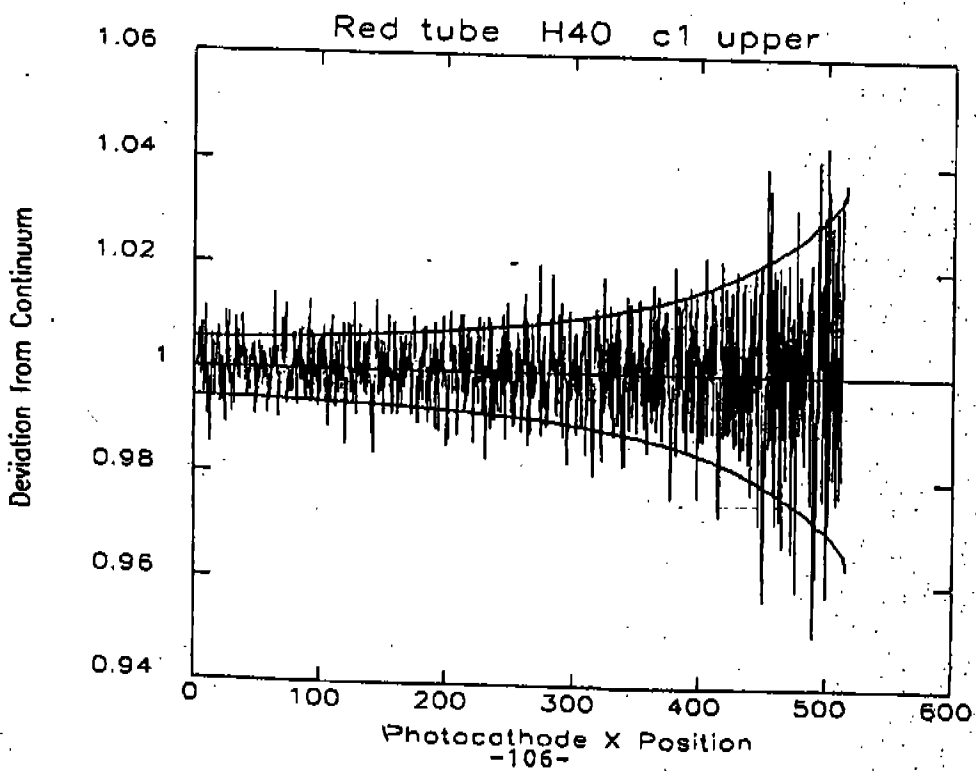
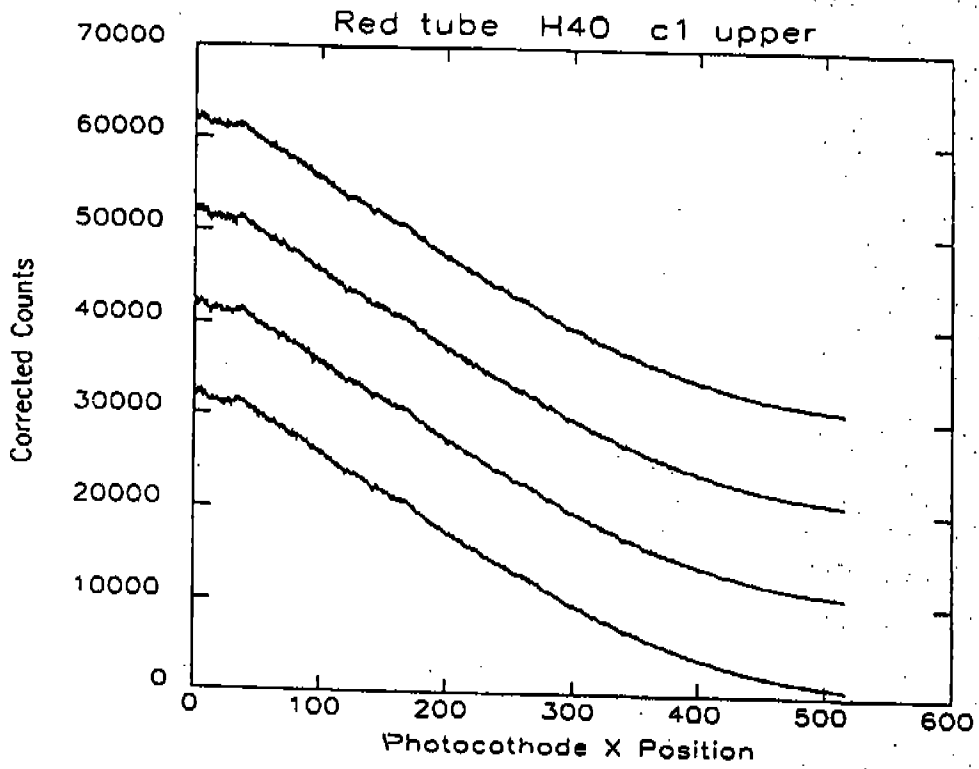


FIGURE 6.1-3

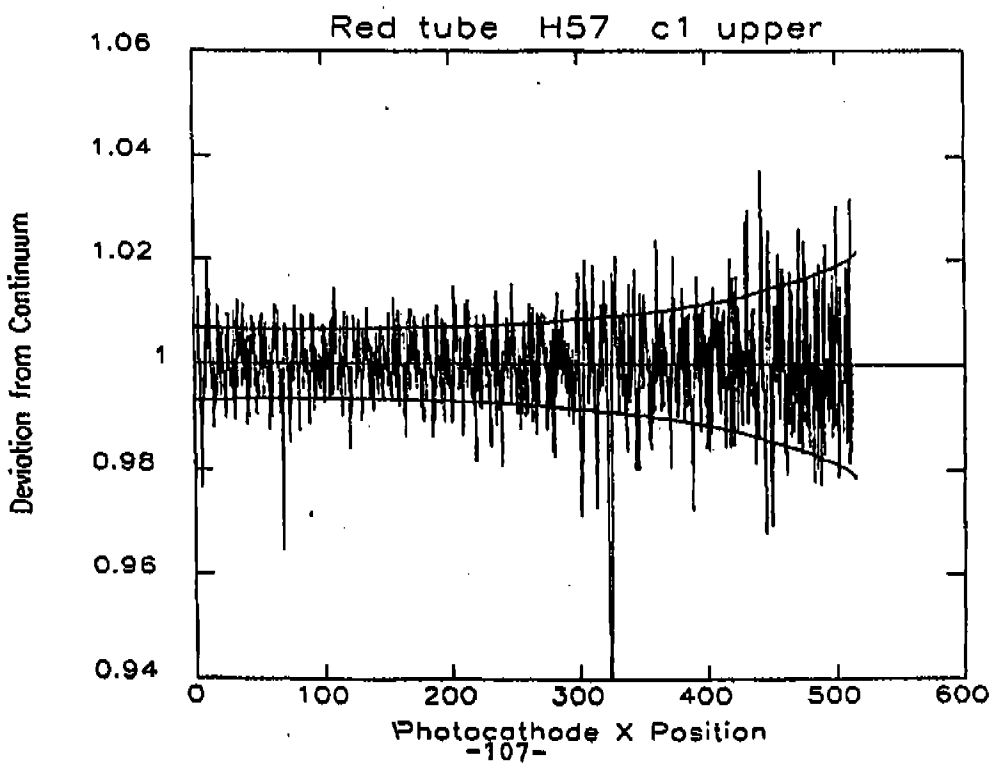
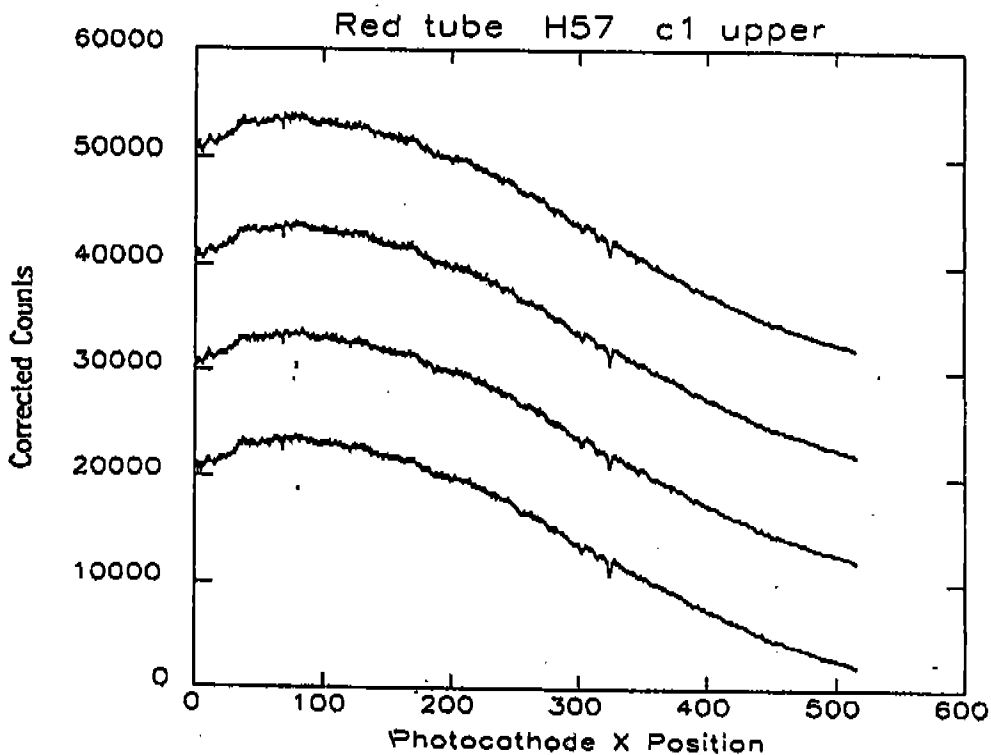


FIGURE 6.1-4

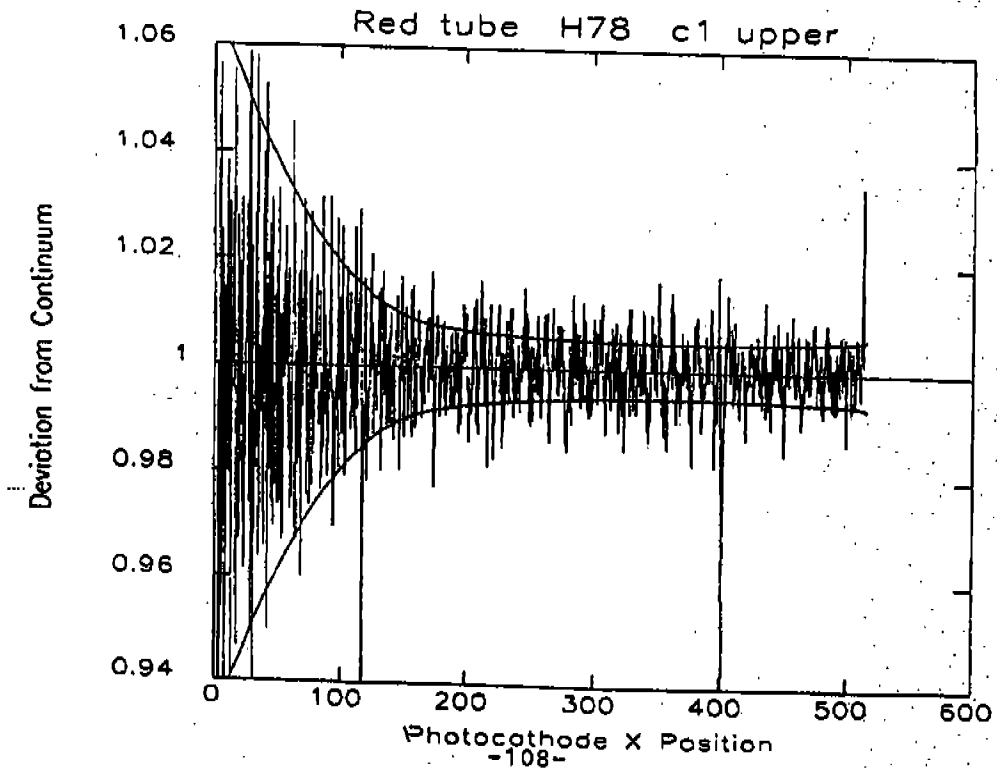
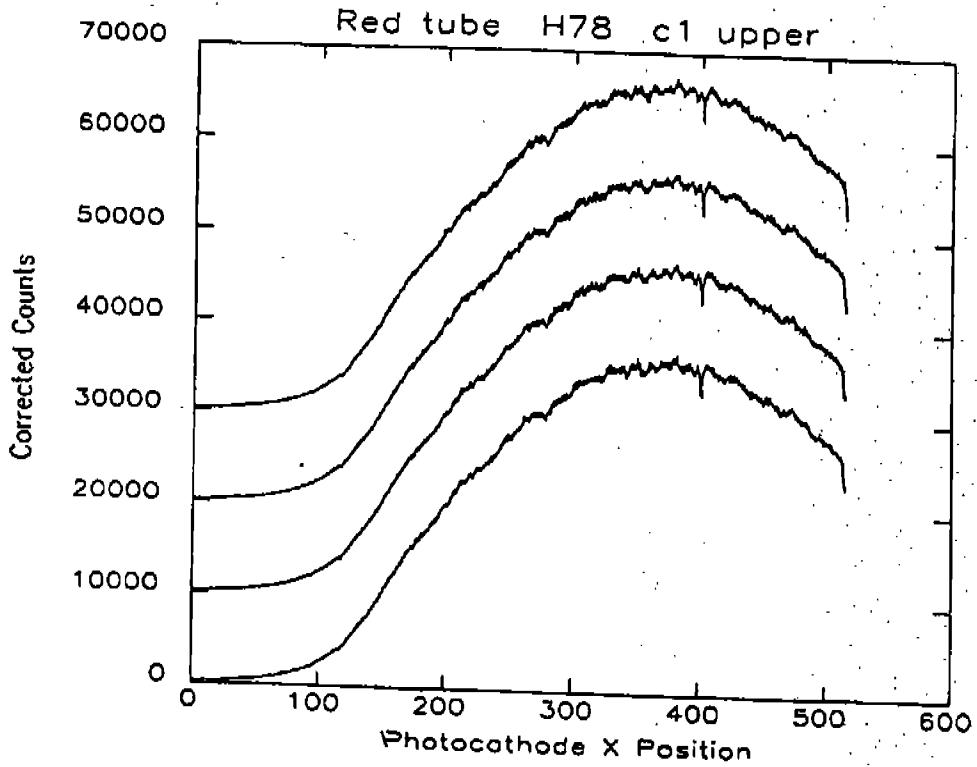


FIGURE 6.1-5

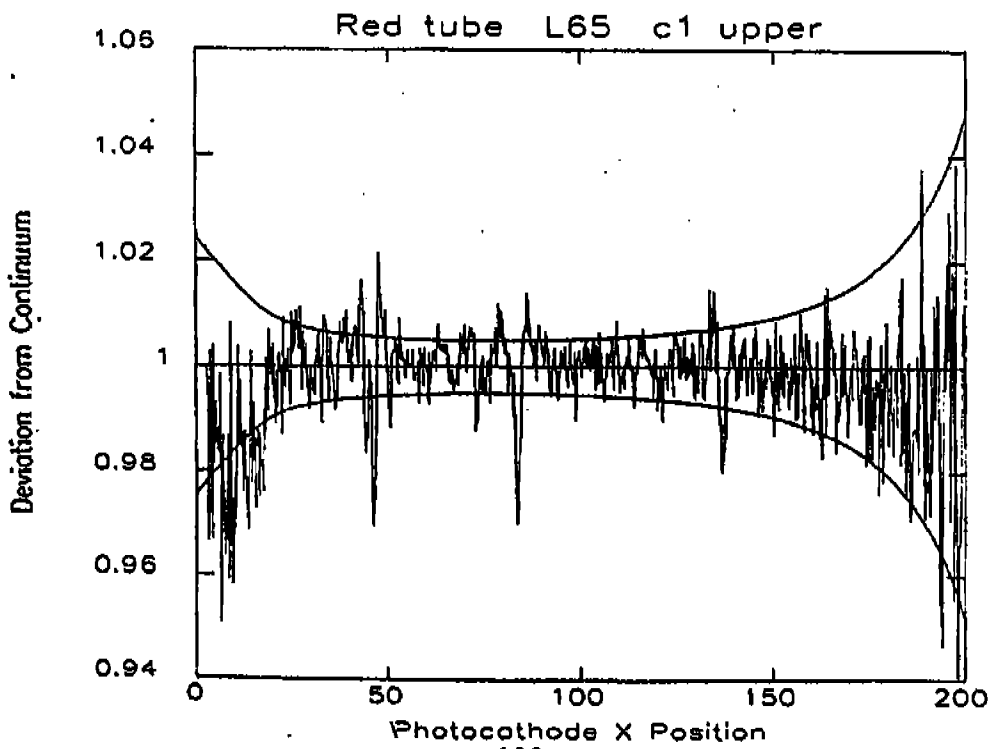
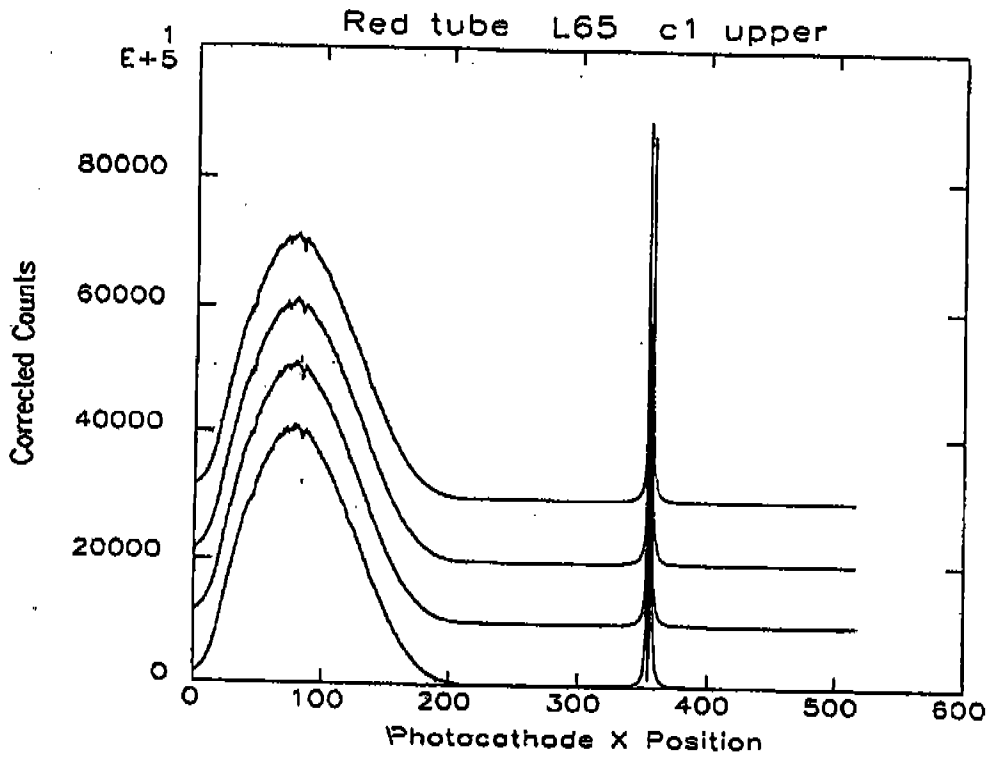


FIGURE 6.1-6

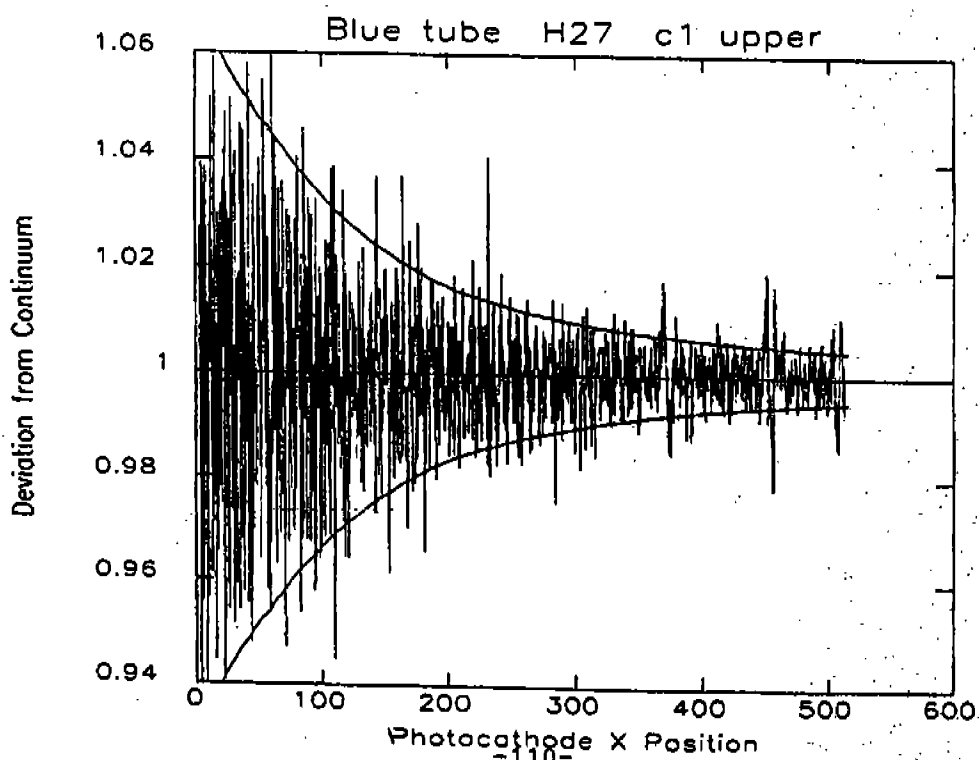
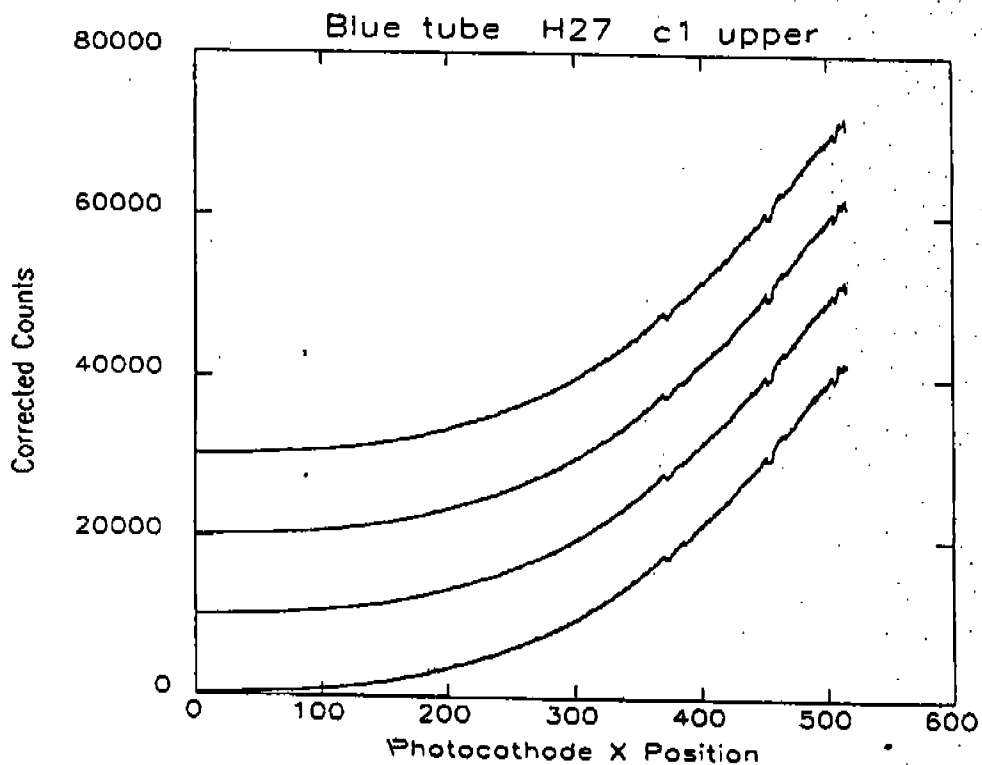


FIGURE 6.1-7

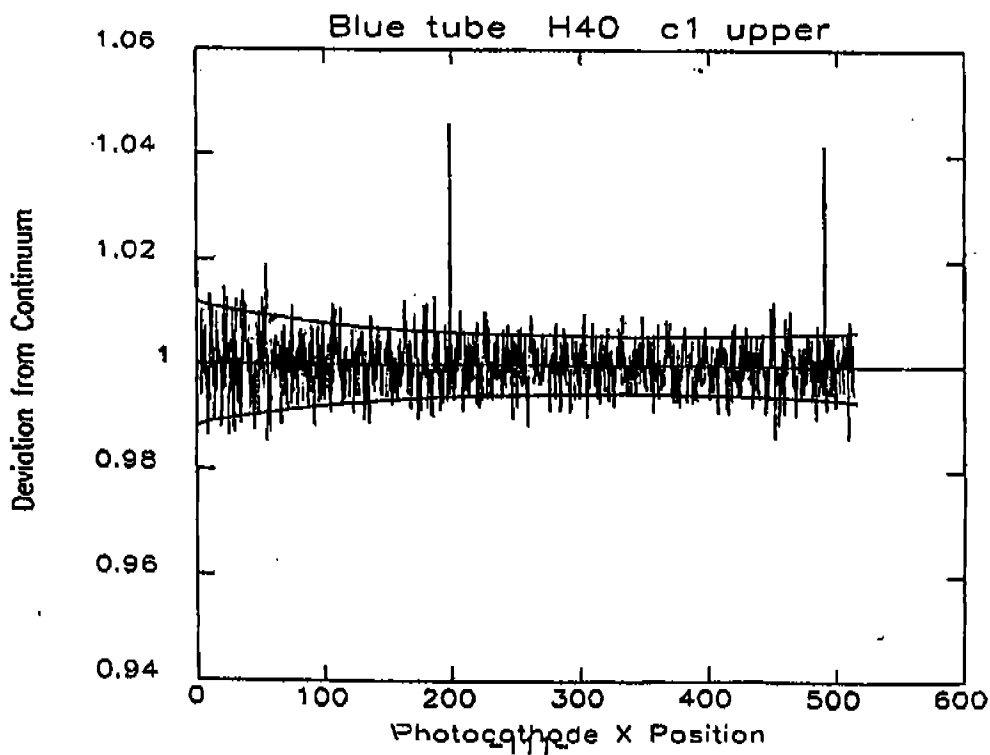
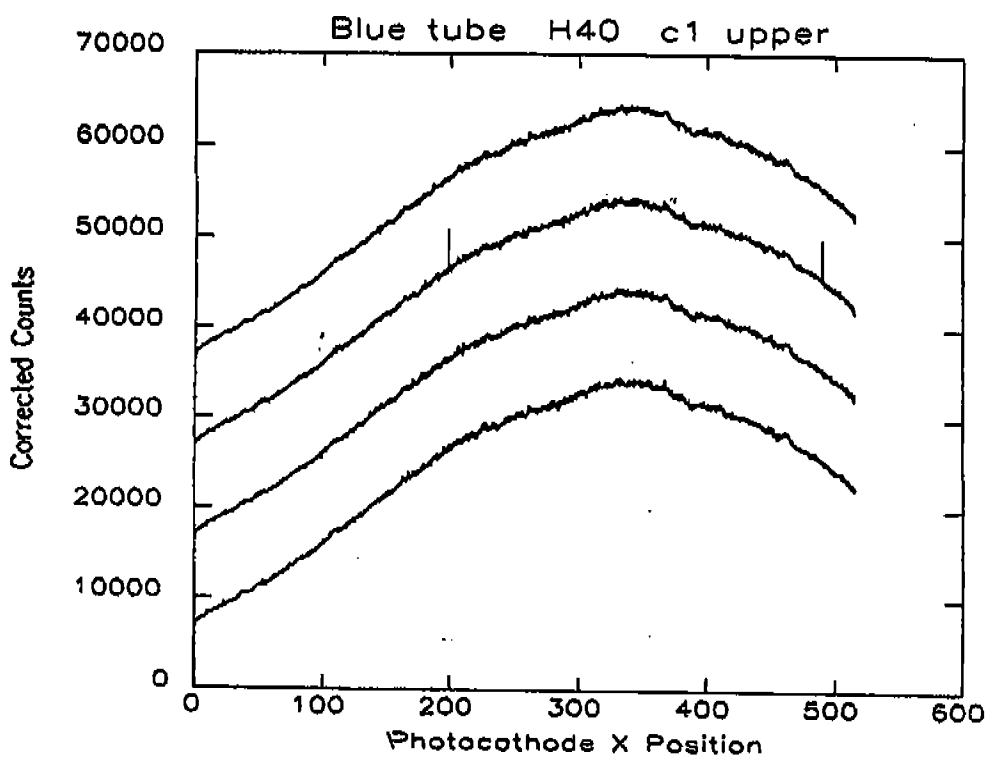
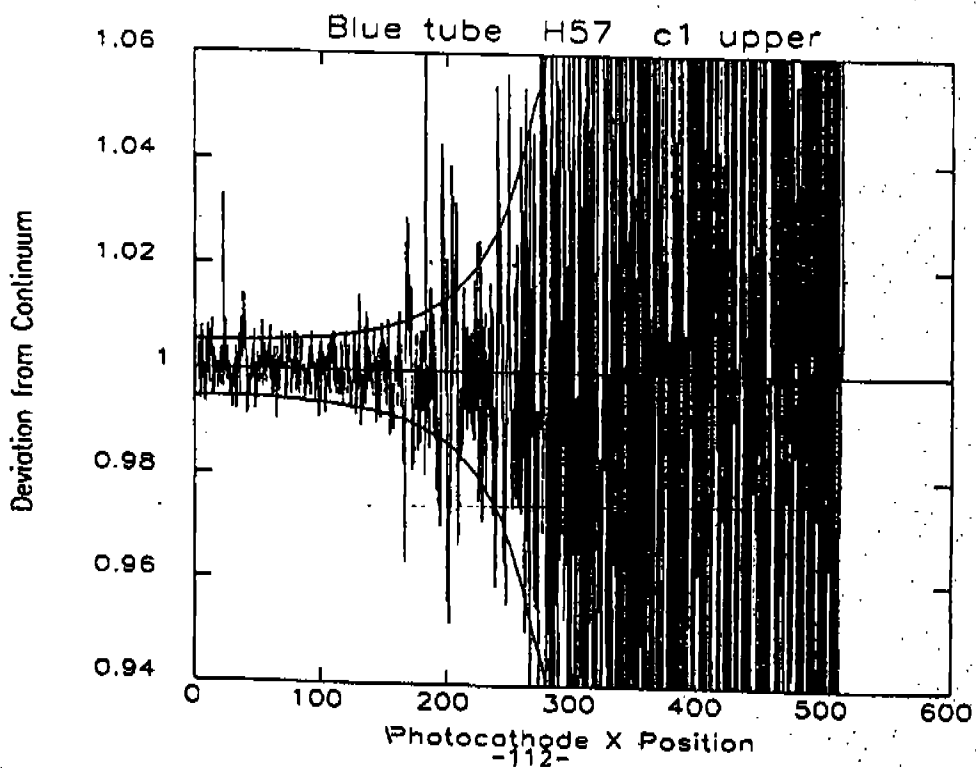
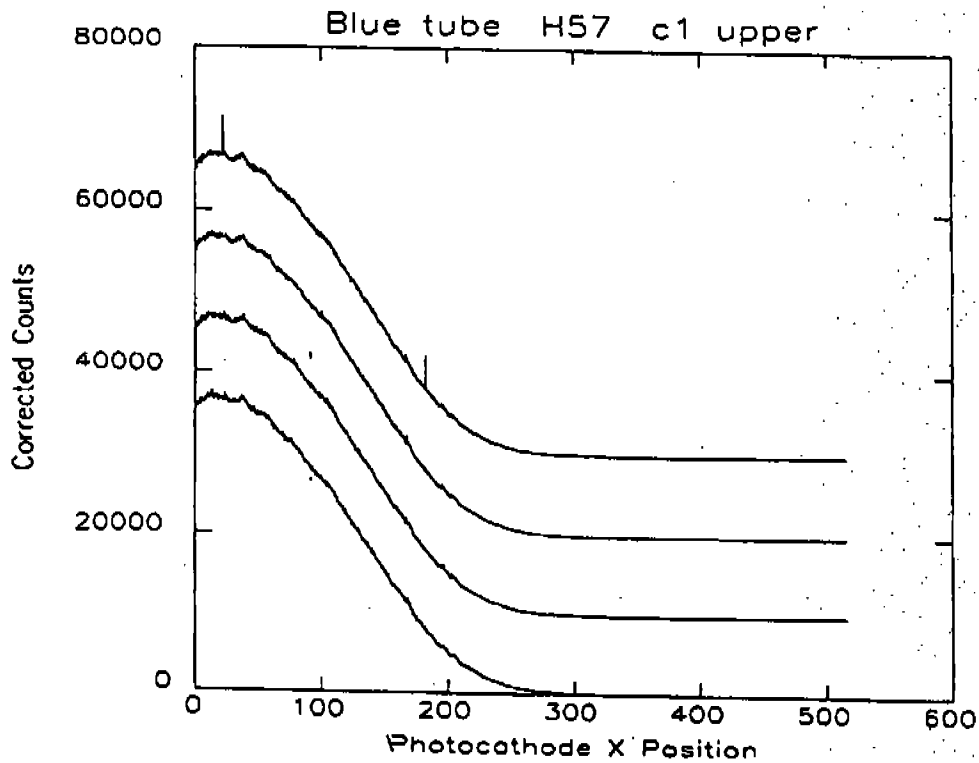


FIGURE 6.1-8



by 10,000 counts. The bottom plots show the deviation of the spectral data from the continuum after summing all four slices. The continuum was estimated by smoothing the data with a 25-point median filter followed by a 15-point mean filter done twice. Also shown are the deviations expected due to counting statistics. The plus and minus two sigma levels are plotted, where sigma is one over the square root of the counts in the continuum. The photocathode X-position in all plots is in 50 micron units (the separation between diodes). Since quarter stepping was used, the separation between data points is 12.5 microns.

Most of the deviation from the continuum is due to the counting statistics. Regions where a large number of counts are available indicate the photocathode granularity is less than 1% in both tubes.

No blemishes were found in the blue tube and the following blemishes (deviations 5%) have been identified in the red tube.

H27 C1 upper - 2
H27 C1 lower - 1
H57 C1 upper - 1
H57 C1 lower - 2
H78 C1 upper - 2
H78 C1 lower - 1

Selected blemishes are shown in Figures 6.1-9 and 6.1-10. The spatial extent of the blemishes along the diode array range from 50 to 250 microns.

During July and August, 1984, a comprehensive set of flat field data was taken for both detectors. Further analysis of these data is needed in the following areas:

1. A complete blemish analysis for all apertures.

FIGURE 6.1-9

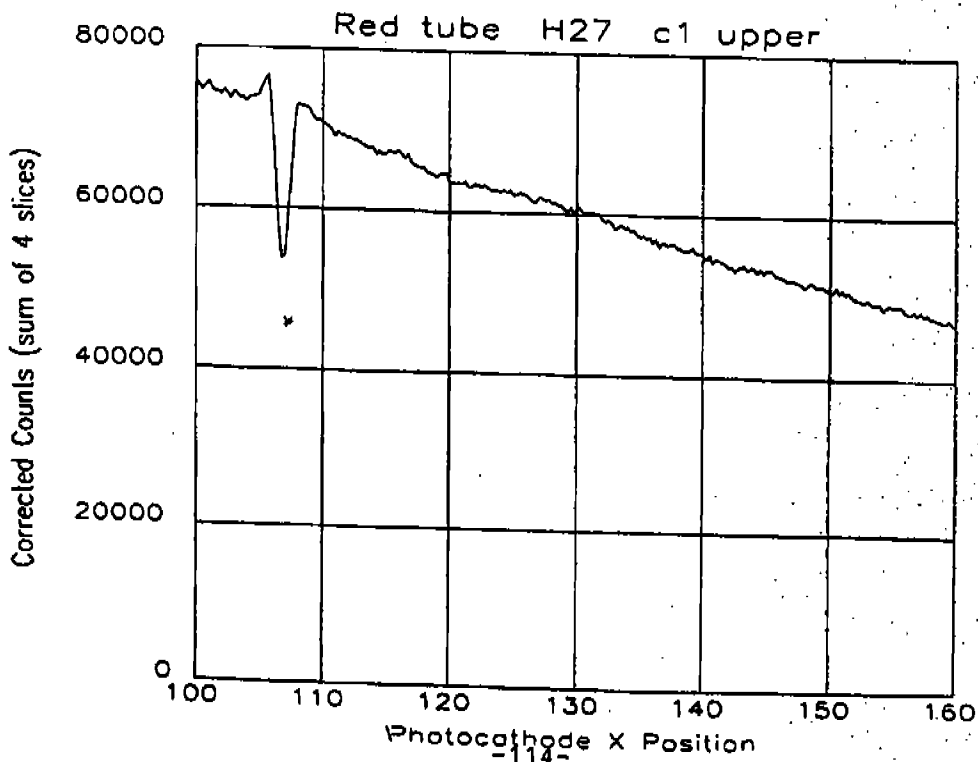
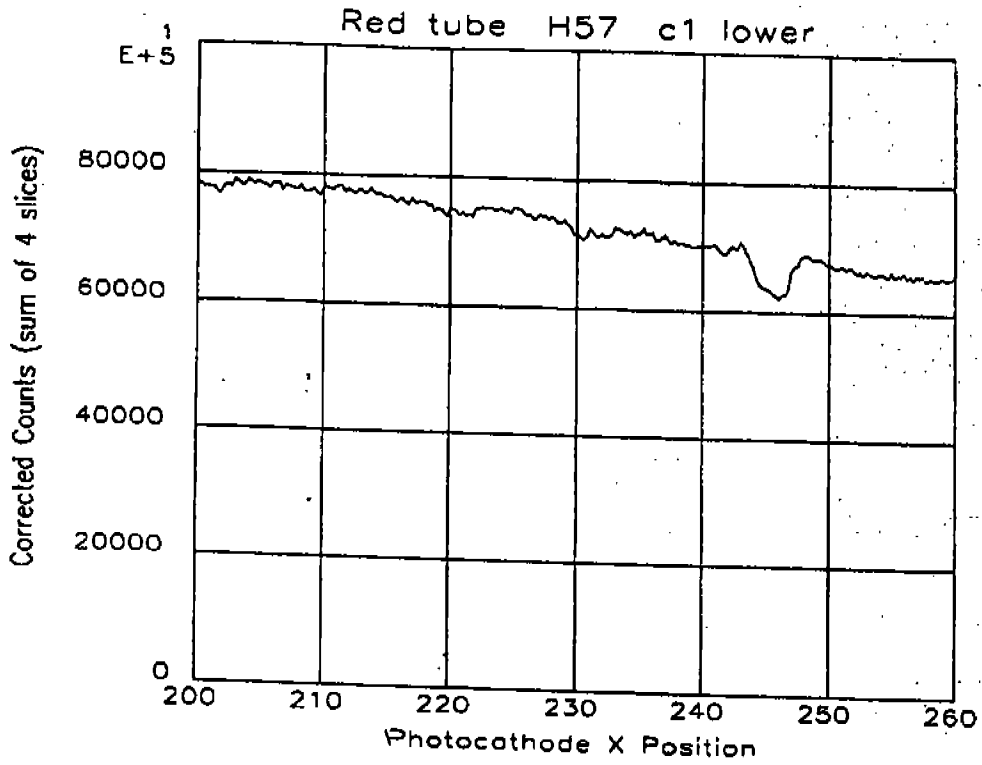
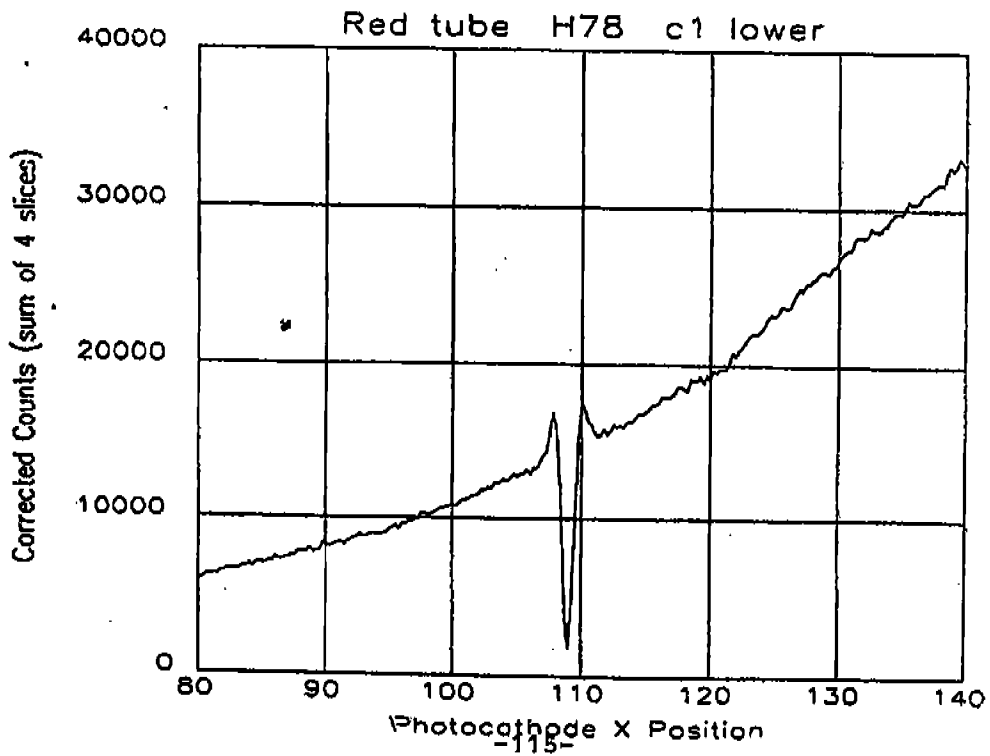
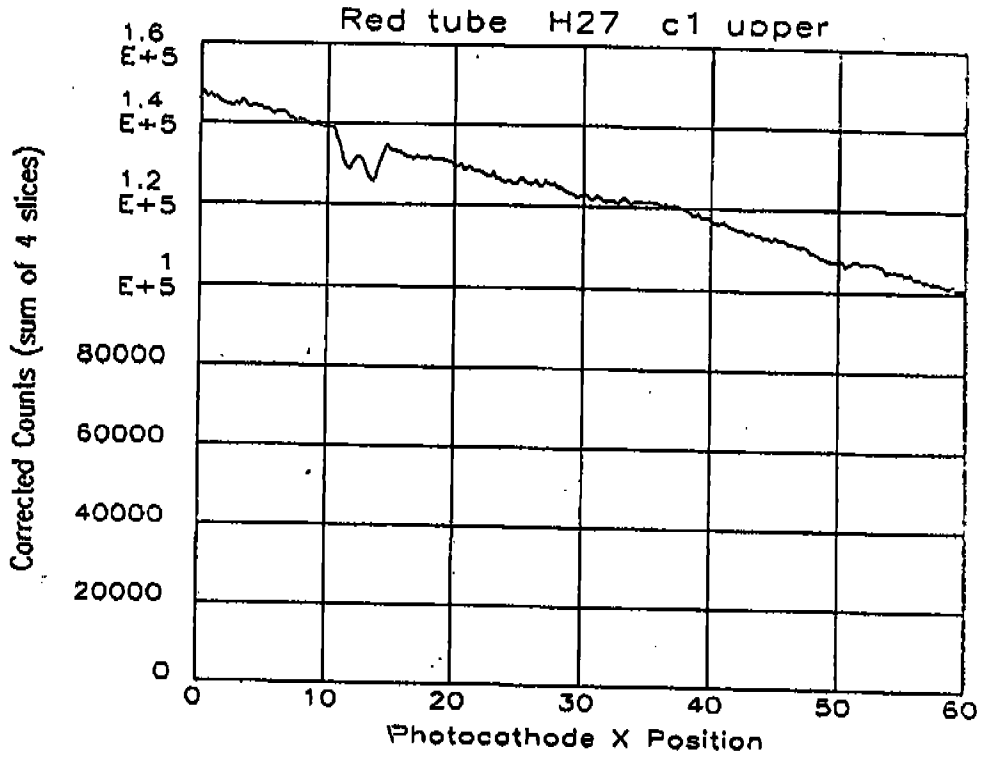


FIGURE 6.1-10



2. Determination of the flat field repeatability, particularly at blemish locations.
3. Analysis of the usefulness of the on-board flat field lamps for determination of the photocathode pixel-to-pixel response and for mapping blemishes.

This laboratory calibration is essential for reduction of flight data, because features in all astronomical calibration sources will complicate blemish analysis. For apertures larger than 0.2 arcsec, the avoidance of blemishes is especially important, because lab calibration spectra are for full aperture illumination, which differs from the vertical extent of the point sources to be observed in flight. A flat field analysis is required for all dispersers and all apertures, because each combination illuminates the photocathode differently in position or extent perpendicular to the dispersion.

6.2 Absolute Instrument Efficiency

A synopsis of recent measurements of the FOS absolute spectrophotometric efficiency in most of its optical configurations is presented. These measurements are compared with those predicted on the basis of earlier evaluations of the efficiencies of the individual components: mirrors, dispersers and filters, and the Digicon quantum efficiencies. Some evidence for degradations in performance is present, although this is not demanded by the data, since discrepancies between the predicted and measured throughput are within estimates of the associated error. Final

estimates of the current FOS throughput for each disperser are included.

6.2.1 Introduction

We present a detailed summary of the relevant measurements which have been made to date in order to estimate the absolute photometric efficiency of the FOS in its standard high and low resolution spectrophotometric modes. The FOS efficiency for spectropolarimetry is discussed elsewhere. The determination of the FOS quantum throughput efficiency (QT) is an indirect process involving several sequential calibrations, each with associated measurement error resulting from statistical fluctuations, as well as systematic effects. While estimates of the statistical uncertainties can be made with confidence, the degree to which systematic effects degrade the calibration is generally difficult to estimate. Where possible several independent measurements of the QT have therefore been made in order to increase the confidence level and to provide indications of the extent to which systematic errors affect the results.

The QT has been determined in two separate ways: 'end-to-end' calibration against previously calibrated standard light sources and from convolution of the individually measured efficiencies of the optical components and the detector quantum efficiencies (QE). The former method involved the design, construction, and absolute calibration of two devices called the Ambient and the Vacuum Space Telescope Optical Simulators (ASTOS and VSTOS). These provide a means of illuminating the FOS in a manner similar to that of the ST, with continuum and spectral

line light sources covering the entire wavelength range over which it is sensitive ($\sim 1200 - 8500 \text{ \AA}$). The ASTOS and VSTOS and their absolute calibrations at the NBS are discussed in the next section and their applications to determine FOS QTe are described in Section 6.2.3. The individual component measurements are briefly described in Section 6.2.4. An analysis and intercomparison of the calibration data are presented, followed by our final estimate of the actual FOS QT for each spectrophotometric mode in Section 6.2.5.

6.2.2 The Space Telescope Optical Simulators (STOSs)

Two separate devices were designed and constructed by MMDA specifically for the FOS throughput measurements: the ambient STOS (ASTOS), for use in air at wavelengths above 2000 \AA , and the vacuum STOS (VTOS), providing illumination sources in the far ultraviolet (FUV). Each was calibrated at the NBS (at separate facilities) both before and after the FOS calibration to assure that significant changes did not occur in their spectral irradiance at the FOS entrance aperture plane, or at least permit an estimate of the uncertainties in the FOS measurements due to such fluctuations. Description of each of these devices, their calibration methods, and uncertainties in the irradiance determinations are discussed separately for each STOS in the following sections.

6.2.2.1 The ASTOS

The ASTOS is the simpler of the two simulators, consisting basically of a means of supporting a light source in front of a barium sulfate coated diffusing screen situated at an appropriate

distance from the FOS entrance apertures. A circular aperture with a central occulting disk is positioned so as to limit the solid angle of diffusing screen seen by the FOS to an f/24 beam with 14% obscuration, mimicking the ST. Either a 1000W tungsten 'FEL' lamp or a gamma scientific deuterium lamp may be used to cover the spectral region from 2000 to 8500 Å. A more detailed description of the ASTOS may be found in Appendix A.

6.2.2.2 ASTOS Calibration

6.2.2.2.1 Method

The ASTOS was calibrated in December 1982 and September 1984 at the FASCAL facility at the NBS in Gaithersburg, MD, by Mr. James Walker under the auspices of Mr. Donald McSparron. The same methods were employed for both calibrations although some improvements in automatic data acquisition capability were made in the interim. The calibrations were performed in two parts: above 3000 Å, the ASTOS spectral irradiance with each of two FEL lamps installed was measured directly by comparison with a 'shelf standard' FEL lamp whose irradiance had been previously calibrated against a black body source. The ASTOS irradiance was too weak below 3000 Å for accurate measurement in this configuration, which employs an integrating sphere in front of the monochromator entrance slit, so for shorter wavelengths (including all of the D₂ lamp measurements), the ASTOS radiance was measured and the irradiance calculated from the geometry. The irradiance calculated in this way was found to agree to within ~2% with the direct irradiance measured at 4000 Å. The same special power supply was used, without adjustment, for each of

the D₂ lamp measurements, so the lamp operating current was presumably constant throughout the calibration period. The FEL lamps were operated nominally at 8.000 Amps, but because of several failures of the Optronics power supply requiring the use of alternate supplies and the use of several different shunts and voltmeters to determine the lamp current, there exists an uncertainty of about 10 mA in the operating current during various phases of the calibration. The September 1984 NBS calibrations were performed at 8.010 A, since this is the current produced by the supply at the setting used for the FOS calibrations (as measured by the NBS), and is most probably representative of the actual lamp current during the August FOS APC measurements. The difference in irradiance between these two operating currents amounts to at most 2% at the shortest wavelengths used and is typically <1%, a small fraction of the estimated uncertainty in the ASTOS calibration. Details of the measurements and the techniques whereby the ASTOS was aligned with the monochromator are given in the NBS Report of Calibration, in Appendix C of this report.

6.2.2.2.2 NBS Results

The measured ASTOS irradiances are also included in Appendix C. The results of interest are those for the FEL lamps GS179 and GS180, and D₂ lamp DL116, each with diffuser #2, since these are the components used for actual FOS absolute photometric calibration APC measurements. The agreement between the 1982 and 1984 FEL lamp calibrations is excellent; discrepancies are typically less than 2% for GS179 and 4% for GS180, and well within the

stated uncertainties which range between 5% and 8%. This agreement extends over the entire wavelength range from 2500 to 9500 Å.

The agreement for the D₂ lamps is not nearly so good, particularly at short wavelengths. An investigation into the cause of the discrepancies led to the discovery of an error in the technique used to calibrate the radiance standard at short wavelengths, involving incorrect dark current subtraction, and the realization that at 2000 Å approximately 95% of the signal is due to scattered light. The former difficulty was corrected with a careful recalibration of the standard, but the scattered light problem caused the estimated uncertainty at 2000 Å to be raised to a factor of 3, at 2100 Å to +30%, and at 2500 Å to +8%. These revised uncertainties still do not account for all of the discrepancy between 1982 and 1984 calibrations, and we suspect that the lamp may suffer variations in intensity and/or spectral distribution.

6.2.2.3 The VSTOS

6.2.2.3.1 Design

The vacuum STOS is a more intricate device than the ASTOS, since it must be capable of repeatedly positioning a number of light sources (the FUV sources tend to cover a fairly limited wavelength range) in such a manner as to properly simulate the illumination from ST, while operating in a vacuum chamber. This is accomplished by a motorized carousel which carries the following lamps: two Pt-Cr-Ne hollow cathode lamps (of the same type used on board the FOS for wavelength calibration, but with

flat MgF_2 windows in place of the lenses used on the FOS lamps), a Quantatec krypton dimer lamp, a Quantatec hydrogen lamp, and a Resonance, Ltd. argon dimer lamp. The latter three provide smooth continuum spectral distributions, while the hollow cathode lamps, one of which has a MgF_2 diffuser (8 microns surface roughness, one side) installed over its window, provide spectral lines which span the entire wavelength range of interest. The source volume of the selected lamp is imaged by a small, inverted Cassegrain telescope, with MgF_2/Al coated mirrors and central obscuration ratio matching ST, onto the FOS entrance apertures with an f/24 beam. A motorized polarizer which can efficiently plane-polarize the beam at a range of angles in 22.5 degree steps is also included. The carousel and polarizer are actuated by means of a special control box. A more detailed description of the VSTOS may be found in Appendix B.

6.2.2.3.2 VSTOS Performance

Because of the focused nature of the VSTOS beam and the fairly small size of the lamp images, it is inherently susceptible to producing variations in the flux seen by the FOS as a result of carousel non-repeatability, misalignment with the FOS, and lamp source volume migration. These possible sources of error in the FOS APC are exacerbated by the nonuniform, sometimes highly asymmetrical, spatial flux distribution of the VSTOS images; furthermore, this distribution was found to have strong wavelength dependence for some lamps. Not surprisingly, the flux levels were also found to vary, especially for the continuum lamps, and the degree of variability is also dependent on wave-

length. Some evidence exists that the rate of variation may be dependent on the lamp use duty-cycle. Some of these difficulties were not apparent at the outset, but were discovered while the APC was in progress. Nevertheless, we believe that a useful calibration of the FOS blue side UV efficiency has been obtained with the VSTOS by careful alignments and judicious choice of data, based on measurements and estimates of the degree to which these deleterious effects operate.

6.2.2.3.2.1 Carousel Repeatability

For the reasons stated above, the VSTOS lamp carousel must be capable of very accurately and repeatably positioning the lamps on the axis of the imaging optics. Tests have shown that the carousel is quite repeatable if undisturbed and if the multiple lamp power cables, which must be free to rotate with the carousel, are carefully draped, so as not to bind or cause excessive torque. This has been possible in practice throughout the calibrations procedures, although some difficulty was encountered with proper actuation of the reset fiducial switch. Small changes in wheel balance and cable-induced torque could change the stepper motor phase at which this switch was actuated, causing each lamp to be positioned one motor step off axis thereafter. Since one motor step moves the lamp image by a significant fraction of its width, a means of mitigating this sensitivity had to be devised. This took the form of an LED on the control panel to indicate when the correct motor phase had been achieved at reset (added during the May 1964 NBS calibration) and the addition of single step control of the carousel

(installed at MMDA prior to the FOS vacuum calibration in July 1984: T/V 3). The carousel is also susceptible to a misphasing if it is manually rotated by one or more turns from the orientation in which it was aligned. This is because the gear ratio between stepper motor pinion and carousel gear does not provide an integral number of motor steps per carousel revolution. Care was generally taken in this regard, but evidence exists that such a misphasing occurred when the VSTOS was mounted and aligned with the FOS just prior to T/V 3. Single step mapping of the lamp images with the FOS showed that the image centers were approximately one step off of the nominal position. Calibration data were subsequently obtained by single-stepping each lamp to its approximate image center.

6.2.2.3.2 Spatial Distribution of Lamp Flux

The image of each of the five VSTOS lamps was carefully mapped with a silicon detector when the lamps were initially aligned prior to the first NBS calibration. The detector window was coated with sodium salicylate to enhance its UV response. In general, the light distribution in the images was found to be fairly symmetrical and broad enough that reasonable care in alignment would yield a satisfactory calibration. After the addition of the carousel single-step capability, we were able to map the images in the FUV (during T/V 3). These data demonstrated that, especially for the argon lamp, the FUV flux distribution is markedly different from that in the visible and near UV, indicating that these emissions are produced in different regions of the lamp. The argon FUV image was found to

be grossly asymmetric and displaced from the center of the image at longer wavelengths. The Kr lamp also exhibited an FUV flux distribution different from that in the visible. More detailed UV mapping in both vertical and horizontal axes was performed during the NBS recalibration of the VSTOS; the results are shown in Figures 6.2.2.3.2-1. The hollow cathode lamps have no obvious wavelength dependence in this regard (as expected) and the diffused lamp has a very broad distribution, making it particularly insensitive to alignment errors.

6.2.2.4 VSTOS Calibration

The VSTOS was calibrated at the NBS by a team consisting primarily of Drs. Jules Z. Klose (NBS), Merv Bridges (NBS), George Hartig (STSCI) and Mr. Elder Constable and Mr. William Miles (MMDA). The consultation services of Dr. Henry Kostkowski were also employed. Separate calibrations were performed in late May and early August 1984, bracketing the FOS T/V 3 APO.

6.2.2.4.1 The NBS Vacuum Calibration System

The apparatus used for VSTOS calibration consists of a one meter Seya-Namioka vacuum UV monochromator with 1200 gr/mm concave grating, an EMR 541F-09-18 CsTe cathode photomultiplier tube (operated at 1900V), a picoammeter, and chart recorder. This was used to compare the spectral irradiances of the VSTOS with argon arc sources of known irradiance in the wavelength range from 1200 to 3000 Å. There exists a fundamental mismatch between these sources however: the VSTOS produces an f/24 beam with 34% (diametrical) obscuration, while the argon arc sources provide much more collimated beams. Furthermore, the monochro-

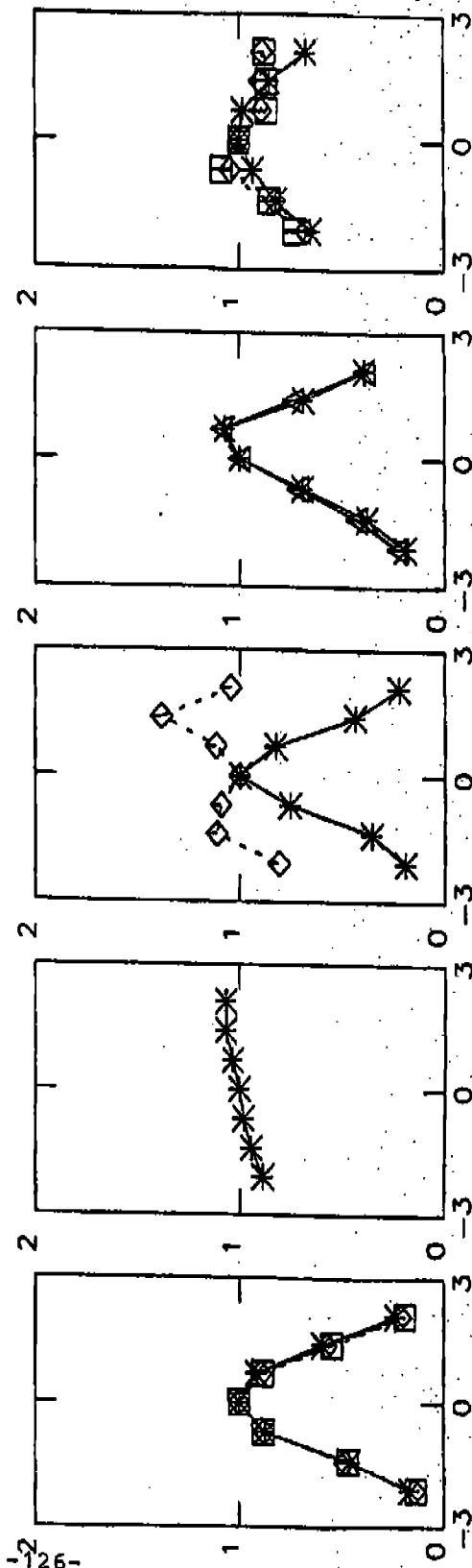
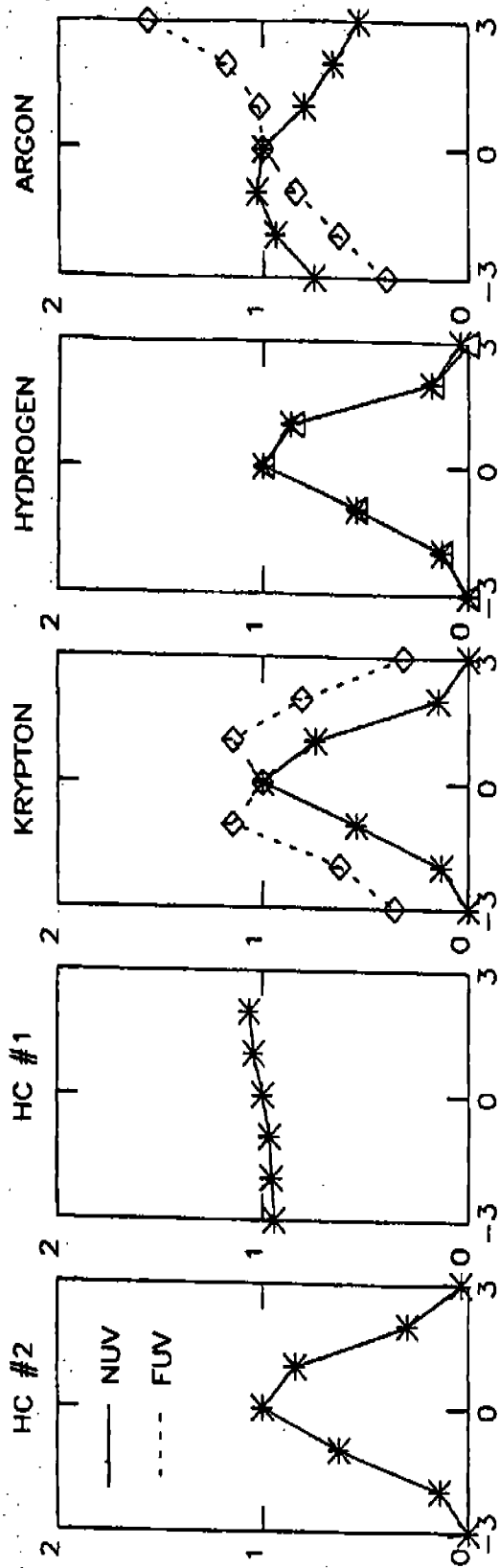


FIGURE 6.2.2.3.2-1. NBS Mapping of VSTOS Images

mator grating was found to be masked such that it would not accept the full VSTOS beam. A new mask was made to alleviate this problem, but it was later discovered that the high degree of astigmatism of the Seya mounting, combined with the small (~9.5 mm diameter) active area of the PMT photocathode, effectively limited the beam to about $f/30$. A careful mapping of the relative response of the monochromator at a variety of wavelengths was thus required in order to properly compensate for the partial beam loss and non-uniformities in grating and photocathode efficiency. We note that this method represents a departure from the standard method for irradiance calibration, in which a diffuser is placed behind the monochromator entrance aperture to avoid beam mismatch problems; however, the VSTOS flux levels, especially at short wavelengths, precluded this approach and necessitated the mapping.

6.2.2.4.2 Calibration of the NBS Monochromator

The NBS monochromator was calibrated (PMT current out vs. spectral irradiance incident on its entrance aperture) in June-July 1984, following the May 1984 VSTOS measurements and again in August, immediately following the VSTOS recalibrations. Measurements were made with both 0.5 and 1.0 mm circular entrance apertures, with 0.5 and 1.8 mm exit slit widths, respectively, matching the configuration used for the VSTOS. The 1 mm aperture remained fixed to the entrance slits of the monochromator throughout the May-August calibration period to eliminate possible errors (due to system nonuniformities) that might arise if its registration were altered. The 0.5 mm aperture, when

required, was registered as well as possible, with the aid of a needle, with the center of the 1 mm aperture.

6.2.2.4.2.1 Method

The calibration was performed, from 2000 to 3100 Å, with an argon mini-arc, designated 'NBS-5', which had been previously calibrated as an irradiance standard (in March 1983) against an argon maxi-arc radiance standard following the method described by Ott, Bridges, and Klose (1980). Briefly, the known relative spectral flux distribution of the radiance source is used to calibrate, on a relative scale, the irradiance of the mini-arc. This is put on an absolute scale by comparison with a tungsten halogen 'FEL' lamp (designated 'F-66') calibrated irradiance source, at the longer wavelengths, since the geometric factors involved should be independent of wavelength. The mini-arc was not calibrated below 2000 Å, and since the maxi-arc has substantially greater flux (required for accurate calibration at the shortest wavelengths), 'MAXI I' was used for calibration below 2000 Å. The same method was employed, i.e., its known spectral radiance was converted to irradiance at the monochromator entrance slit by comparison with the NBS-5 mini-arc in the region of overlap (above 2000 Å). The original maxi-arc radiance calibration was performed by comparison with a hydrogen arc whose radiance is calculable (Ott, Behringer, and Gieres 1975 and Ott, Fieffe-Prevost, and Wiese 1973).

In each case, the MgF_2 window used to isolate the VSTOS vacuum chamber (and therefore in the VSTOS beam during its measurements) was placed between the arc and the entrance aper-

ture. A cursory mapping of this window, made by moving it around in the (narrow) maxi-arc beam, indicated that its transmittance was quite uniform, so beam size and window position considerations are insignificant. The volume between this window and the monochromator entrance port assembly window (also MgF_2) was flushed with argon during all calibration measurements, and care was taken to assure that no volume of trapped air was present in the lamp/window configurations. (This was a problem in our first attempts to perform the calibration.)

6.2.2.4.2.2 Mapping

Because of the mismatch between the narrow arc beam and the f/24 VSTOS beam, the response of the monochromator at various incidence angles (relative to that on-axis) had to be mapped out. This was accomplished by mounting the maxi-arc on a special fixture, so that it could be rotated horizontally about a point directly beneath the entrance aperture, while jack screws could be turned to do the same in the vertical direction. Mapping was performed over the approximately ± 1.2 degree angles of incidence that define an f/24 beam. Fairly strong wavelength dependence was found, so the mapping was undertaken at 10 wavelengths covering the 1200-3000 Å range. Relatively small variations occurred as the beam was moved horizontally, but strong dependence on vertical angle was evident. This is interpreted as evidence that the grating efficiency is fairly uniform, but the PMT photocathode response varies markedly as the image is moved up and down along the monochromator exit slit. Mapping was performed only along the axes (which intersect at the monochro-

mator optical axis), the efficiency at other points in the beam was assumed to be sufficiently well represented by the product of the efficiencies at corresponding points on the axes. Then, assuming a perfectly uniform distribution of flux in the VSTOS beam, the monochromator response to its f/24, centrally obscured beam was calculated relative to the maxi-arc beam on-axis. This result, shown in Figure 6.2.2.4.2-1, was then applied to the monochromator calibration to estimate its true response to the VSTOS beam.

6.2.2.4.2.3 Calibration Uncertainties

The signal levels involved for all of the argon arc calibrations are high enough that system noise is essentially negligible, and statistical uncertainties are dominated by our ability to read the chart recordings; typical accuracy is $\pm 2\%$. The NBS-quoted uncertainty in the absolute radiance calibration of the MAXI-I arc ranges from $\pm 5\%$ above 1500 \AA , degrading to $\pm 10\%$ at shorter wavelengths, where the continuum is contaminated by variable emission lines. The absolute irradiance of the NBS-5 mini-arc is known to within 6% over the interval $2000\text{-}3200 \text{ \AA}$; independent measurements of the arc irradiance in August 1983 and March 1983 agree to within $\pm 2\%$. Systematic errors in the monochromator calibration may also be important, but are difficult to estimate. Some possible sources of such errors are:

1. Misalignment of the arc with the monochromator axis. The mapping of the response allows us to make an estimate of the error due to angular misalignment; estimating that maximum possible such

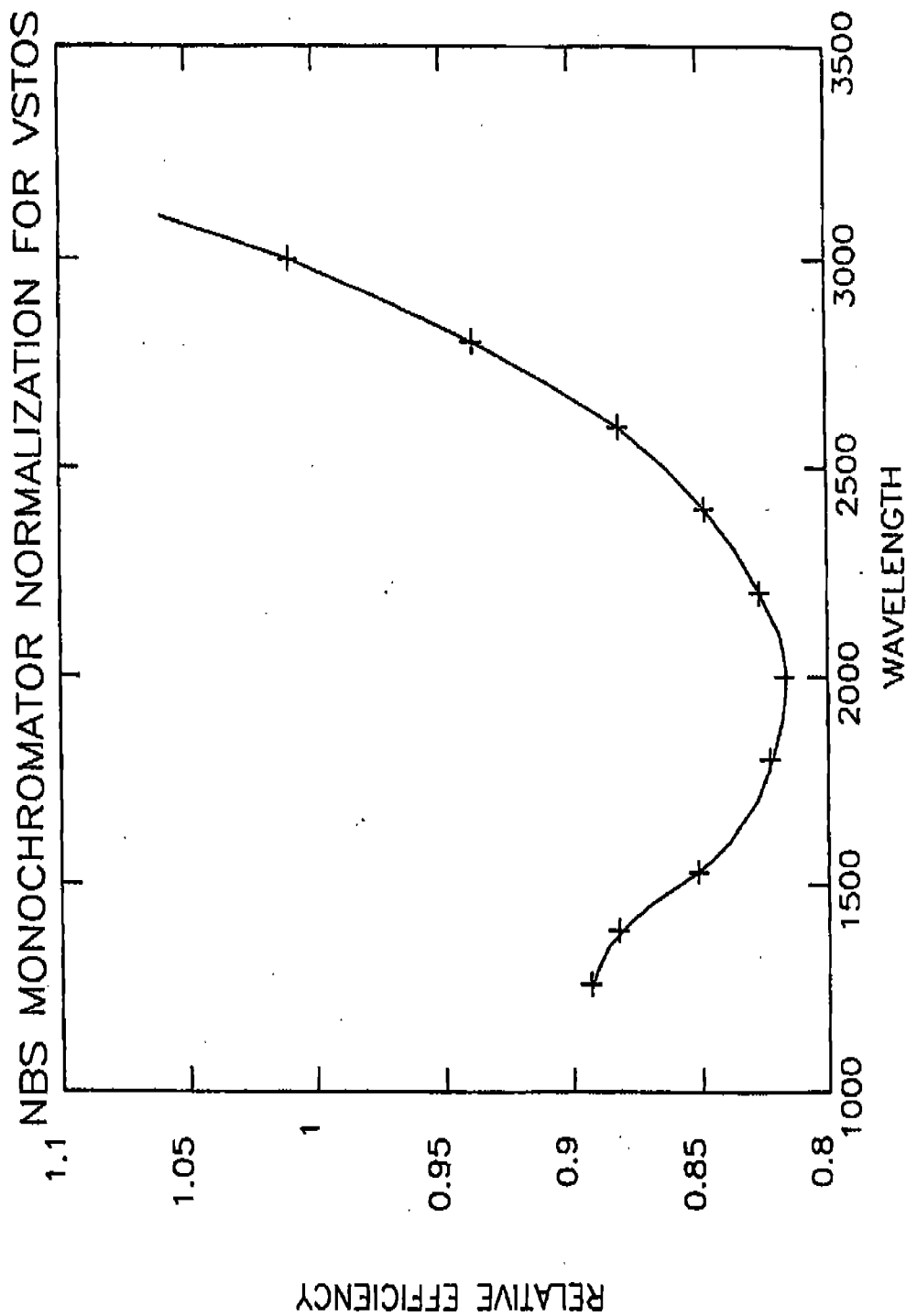


Figure 6.2.2.4.2-1. Relative Response of NBS System to VSTOS Beam

alignment error is less than $\pm 1^\circ$, the uncertainty is $\pm 4\%$. The arc source beams are narrow and nearly collimated, so they must be well centered on the entrance aperture; however, care was taken to maximize the signal (by effect) so this source of error becomes minimal.

2. Non-linearity of the PMT, picoammeter, or chart recorder. The latter two instruments have been calibrated, and we expect error contributions of $< 2\%$. PMT nonlinearity is also unlikely to be a major ($> 2\%$) error source at the currents used for these measurements, since the ratio of the 0.5 mm/0.8 mm and 1.0 mm/1.8 mm entrance/exit slit combinations remained constant over a wide range of PMT currents and were the same for both mini- and maxi-arcs.
3. Improper registration of the 0.5 mm entrance aperture pinholes. As mentioned above, the 1 mm aperture remained in place throughout the calibration, but the 0.5 mm pinhole had to be removed and replaced on numerous occasions. If improperly placed (it was taped over the 1 mm pinholes), some of its area might be occulted (once it slipped causing an obvious measurement discrepancy!). The ratio between measurements in the small and large aperture configuration is just that expected from the relative aperture areas and the spectral

resolutions, so we deduce that this is not a real error source.

4. Arc fluctuations. The NBS-5 arc appeared to be very stable and repeatable throughout the measurements. There is some evidence, however, that the MAXI-I arc suffered some instability and variations in its spectral distributions. In the region of overlap between NBS-5 and MAXI-I calibration spectra, we expect to be able to derive a wavelength independent ratio that can be used to scale the known MAXI-I spectral radiance to irradiance at the entrance aperture. This factor was found to have a wavelength dependence in the sense that ~8% more flux than expected from MAXI-I occurs at the longest wavelengths in the August data. Also, the ratio between the small and large aperture configurations is constant (and nominal) at long wavelengths, but shows an increase below ~ 1600 Å (more flux seen through the small aperture than expected) possibly indicating a change in spectral distribution between these two runs. The maxi-arc also showed visible and audible signs of instability. For these reasons, we suspect that some systematic error may be present in the monochromator calibration below 2000 Å, but have no means of estimating its severity. Comparison of the June/July measurements with the August data

is precluded because the monochromator entrance port window was changed in the interim (resulting in a factor of 15 improvement in throughput at 1250 Å).

Our best estimate of the monochromator calibration uncertainty may be summarized as follows:

1. Above 2000 Å, where the calibration is reliant only on the NBS-5 arc, the measurement uncertainties are ±8%.
2. Below 2000 Å, this accuracy degrades with decreasing wavelengths, to ±10% at 1600 Å and ±15% at 1250 Å.

6.2.2.4.3 VSTOS Configuration and Alignment with NBS System

A special vacuum chamber was provided by MMDA for the purpose of VSTOS calibration. The chamber, pumped by an array of four sorption pumps and a CTI cryopump, was equipped with feed-throughs for the VSTOS control signals, lamp cables, and thermistors and three windowed ports for inspection of VSTOS operation. To assure its cleanliness, the chamber was given an acid bath clean-up and a vacuum bake-out was performed before installation of the STOS. Witness mirrors were also employed. The STOS was mounted on a platform equipped with three jack screws for vertical tilt and translation adjustment and screws for translation in the horizontal and focus directions. Horizontal tilt was adjusted by loosening clamps that attach this entire assembly to the floor of the chamber. The VSTOS beam exited the chamber through an MgF₂ window (which was removed from the chamber and

introduced into the arc beam during NBS monochromator calibration) to which a bellows was attached in order to seal the volume between the tank and monochromator entrance port window. This volume was flushed with argon during all measurements below 2000 Å. All measurements were made with the VSTOS under hard vacuum (chamber pressure $< 2 \times 10^{-5}$ T).

6.2.2.4.3.1 Alignment Method

Alignment of the VSTOS was effected in two steps: a crude alignment was first obtained by means of a laser beam and final adjustments were made by peaking up the monochromator signal. A He-Ne laser was initially aligned with the monochromator by adjusting its tilt until it shone through the centers of both entrance and exit slits and was reflected (in zeroth order) from the exact center of the concave grating. The VSTOS was then adjusted, so that this beam was centered on the back of the secondary mirror support of the VSTOS inverted Cassegrain and was reflected, from a glass plate held flat against the VSTOS front mounting surface, back onto the monochromator entrance aperture. The distance between this mounting plate and the aperture was adjusted to be equal to that in the FOS calibrations configuration (34.8 cm). The VSTOS was then prepared for vacuum operation (all lamp cables attached and carefully adjusted to assure that they would move freely and cover minimal torque on the carousel), the PMT replaced on the monochromator, and the glass plate removed from the front of the VSTOS. The VSTOS carousel was reset, then moved to the Pt-Cr-Ne #2 lamp position and the signal from a strong line maximized by a combination of small tilt and transla-

tion adjustments in both axes. This lamp was chosen for alignment purposes because of its relatively small and symmetrical image. The vacuum chamber was then closed, with the MgF_2 window and bellows installed, and evacuated. Finally, the operation of the carousel and all lamps was checked before proceeding with the calibration.

6.2.2.4.3.2 VSTOS Image Mapping

The image of each of the VSTOS lamps at the (1 mm) monochromator entrance aperture was mapped during the August recalibration to determine the alignment sensitivity. Horizontal mapping was achieved by rotating the VSTOS lamp carousel by single motor steps, moving the image ~1 mm per step. Vertical mapping was done by turning the jack screw under the monochromator entrance port tube, thereby raising and lowering the aperture, while tilting the entire monochromator. Vertical step size was 0.7 mm. Changes in monochromator response due to the very small tilt, as well as changes in the image intensity and spatial distribution due to variation of the source position relative to the VSTOS optical axis, were assumed to be minor over the range of the mapping. Measurements were generally made near both the long and short wavelength ends of the calibrated spectrum of each lamp, to investigate wavelength dependencies. Figure 6.2.2.3.2-1 illustrates the results.

Of particular interest are the strong wavelength dependence of the profiles for the argon and krypton lamps. The FUV profiles for the argon lamp are asymmetrical and displaced from these at longer wavelengths, rendering this lamp less than ideal as an FUV

calibration source. The Kr lamp image is considerably narrower as seen in the UV, and inverted at the center at short wavelengths, but the profiles are at least symmetrical and their center does not shift with wavelength. The images of the hollow cathode lamps and the hydrogen lamp exhibit no significant wavelength dependence. The narrow, symmetrical distribution for the Pt-Cr-Ne #2 lamp make it the ideal choice for the alignment (peak-up) source, while the broad, nearly flat profiles for the Pt-Cr-Ne #1 lamp (with diffuser) make it most insensitive to alignment error and, as such, particularly useful as an absolute calibration standard.

6.2.2.4.4 VSTOS Calibration Method

As was indicated above, the monochromator was used in two configurations, with a 1.0 mm entrance aperture and 1.8 mm exit slit and with a 0.5 mm aperture and 0.8 mm slit. The larger aperture was used to measure all of the VSTOS lamps, while the smaller was used for the Pt-Cr-Ne #2 lamp alone, in order to provide the increased spectral resolution which was required for the separation of sufficient lines in the rather dense line distribution provided by the hollow-cathode lamps. The attenuation produced by the MgF₂ diffuser on the #1 lamp precluded use of the smaller aperture for this lamp, hence its calibration suffers greater uncertainties due to poorer signal-to-signal ratio (lines shortward of 1524 Å could not be measured) and blending. The exit slit width was empirically determined in each case by opening it until the measured flux from an isolated line (from the Pt-Cr-Ne #2 lamp) was maximized, then reducing it to

just the point where the signal began to drop. (Scans were made through the line during this procedure.)

Measurements below 2200 Å were made with the volume between the monochromator entrance port window and the VSTOS chamber window flushed with argon. The critical flow rate was determined by observing the measured flux at short wavelengths, while adjusting the rate (with a flowmeter in the line) and watching for absorption by air diffusing into the cell. Measurements were subsequently made at flow rates significantly larger than this critical value. At wavelengths longward of 2200 Å, air was introduced into the cell, thereby providing an order blocking filter.

6.2.2.4.4.1 Line Source Measurements

The spectral bandpass for each configuration is required for the calibration of the line source irradiances. This was measured by slowly scanning the isolated 2930 Å PtI line and calculating its full width at half maximum intensity. The dispersion of the Seya-Namioka monochromator is not constant, however, so the resolution measured at 2930 Å must be corrected for use at shorter wavelengths. This correction amounts to a 13% increase in $\Delta\lambda$ at 11200; a linear approximation is sufficiently accurate for $\Delta\lambda$ computation at intermediate wavelengths.

Initial measurements of the line fluxes were made by scanning the region around each of the selected lines in order to determine the wavelength of peak signal and determine the degree of blending. Final lines selection was based on the need for a sufficient number of lines to provide adequate coverage over each

of the UV grating ranges (~5 lines, evenly spaced was our goal), the relative amount of blending in the candidate lines, and their intensity.

The Pt-Or-Ne lamps were allowed to stabilize for at least 15 minutes prior to calibration. Some variation (different for each line) does continue to occur after this warm-up period, but this is typically on the order of 5% per hour and is not asymptotic.

6.2.2.4.4.2 Continuum Lamp Measurements

The krypton, argon, and hydrogen lamps were initially scanned over the entire range of the monochromator ($\lambda\lambda 1150-3100$) to determine which portions of their spectra were relatively free of contamination by lines, which tend to be intrinsically variable and also effect the accuracy of the calibration transfer between instruments with different spectral resolution, and had sufficient flux to be accurately measurable. The argon lamp was determined to be useful in the ranges $\lambda\lambda 1200-1450$ and $\lambda\lambda 2200-3000$; the krypton lamp in $\lambda\lambda 1300-3100$ and the hydrogen lamp in $\lambda\lambda 1700-3000$.

The stability and required 'warm-up' time of the continuum lamps were investigated during the May calibration, the latter by rapid rescanning of the spectrum, or a selected portion thereof, while the lamp stabilized after a 'cold' start. Variations in the UV fluxes were observed for all three lamps, but were not major (typically $<\pm 3\%$) after a half-hour or less of operation. The krypton lamp flux continued to drop at a slow rate ($<2\%$ per hour) from the level reached shortly after turn-on. The hydrogen lamp was disappointing in that it often required restarting after

it spontaneously extinguished; such restarts often resulted in fluxes considerably different from those just before failure.

An attempt was made to provide a means of independently determining the state of lamp stability by placing a pair of silicon photodiode/op-amp devices in front of the lamp carousel, such that the integrated flux level of two of the off-axis lamps could be monitored. Despite the fact that the detector windows were coated with sodium salicylate to extend their UV response, the behavior recorded by these monitors was generally not indicative of the UV flux variations measured with the NBS system.

The long-term stability of each of the continuum lamps was quite disappointing. The UV fluxes from both argon and krypton lamps decayed steadily from use to use, always restarting at levels below that recorded just before the previous turn-off. NBS system degradation cannot be at fault for these decays, because they occur at different rates and the Pt-Cr-Ne lamp fluxes remained very constant throughout each calibration. The hydrogen lamp was less predictable and, as mentioned above, its output was dependent on whether or not restarting was required (as was often the case). It was also discovered that repeatedly pressing the 'start' switch for this lamp could change the lamp flux, indicating that it can operate in a variety of modes.

6.2.2.4.5 VSTOS Calibration Results

A summary of the detailed calibration results, including a log of the measurements, may be found in the informal NBS report submitted by Dr. Klose, which is included as an appendix in the STSci Document FOS/CAL-15, Absolute Photometric Calibration of

the FOS, authored by Dr. George Hartig. The logs, in addition to the date, times and configuration for each run, also indicate the signal level at one or more wavelengths to demonstrate the repeatability of each lamp. Since these are raw signal (dark subtracted) measurements, the pre- and post-FOS calibration values cannot be directly compared, because of the replacement of the monochromator entrance assembly window between the May and August calibrations. Of particular note is the stability of the Pt-Cr-Ne #2 lamp throughout each run; the measured signal from all three lines included in the logs is repeatable from day to day within several percent. This attests to the stability of the NBS system and the repeatability of the VSTOS carousel in addition to that of the lamp itself. The other hollow cathode lamp was not monitored so frequently and the diffuser was added in the middle of the May calibration, but those measurements which are available indicate that this lamp is also very stable over periods of tens of hours of use.

Unfortunately, this is not true of the continuum sources. The hydrogen lamp proved to be rather erratic and gave indications of several modes of operation which settle to different flux output levels. Generally, though, the levels reached after 1 hour warm-up were within +8% of the average, especially if a restart was not required. No systematic trend could be discerned. The krypton and argon lamps both exhibited a very clear trend toward decreasing equilibrium flux with continued use. For this reason, logs of the lamp use were kept through the FOS calibration period with hope that a reasonably accurate

interpolation to the actual flux levels at the time of the FOS APC could be made. Figures 6.2.2.4.5-1 and 6.2.2.4.5-2 illustrate the calibration histories of these lamps at wavelengths near the peak of their FUV continua and in the near UV. The trend to decreasing flux with accumulated lamp use is evident during the May calibration for both lamps, and this trend continues during the August calibration for the krypton lamp. The argon lamp behaves more erratically (in the FUV) during the August calibration, and jumps up by about a factor 2.4 between May 31 and August 7. Only a small increase is noted for the krypton lamp at a slightly longer wavelength, so the monochromator calibration is not likely at fault. (Also note that in August the Pt-Cr-Ne #2 lamp lines at 11248 and 11404 each show a decrease of ~30% from their May levels.) At longer wavelengths (e.g., 12300), the argon lamp flux increased by only 20% in the same interval, and proceeded to decrease monotonically during the August measurements, as in May.

It is obvious that the consistent degradations measured during the NBS calibration periods could not have persisted at the same rate, while the lamps were used for the FOS APC; in fact, they seem to have recovered slightly during that period. Therefore, estimation of the flux at the time of FOS APC cannot be made by direct interpolation or extrapolation of the levels shown in Figures 6.2.2.4.5-1 and 6.2.2.4.5-2. It is unclear what degradation mechanism could be operating during the NBS calibrations; it may be dependent on duty cycle, since the lamps were used sparingly with fairly long rest periods between APC measure-

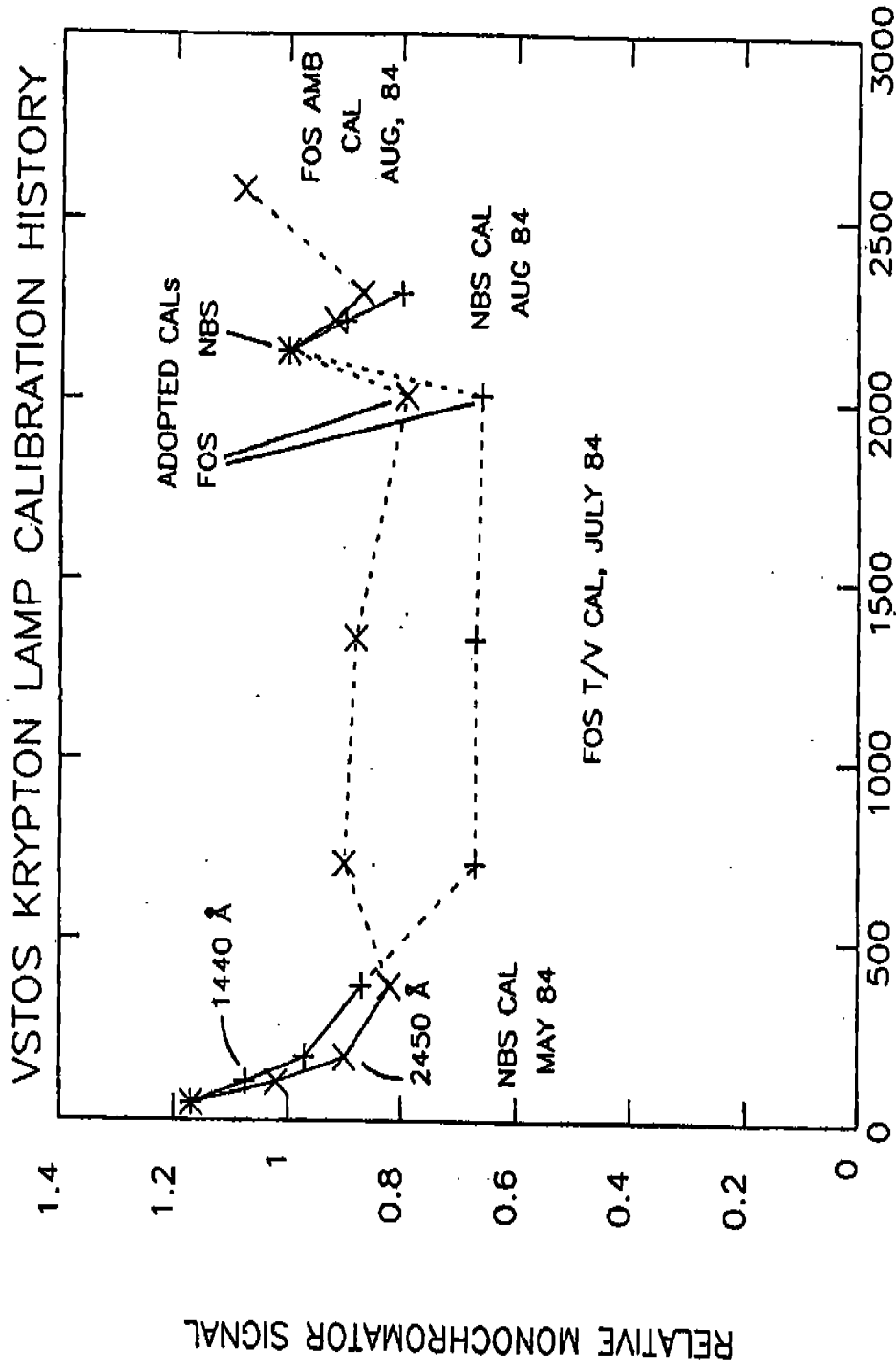


Figure 6.2.2.4.5-1. VSTOS Krypton Lamp Calibration History

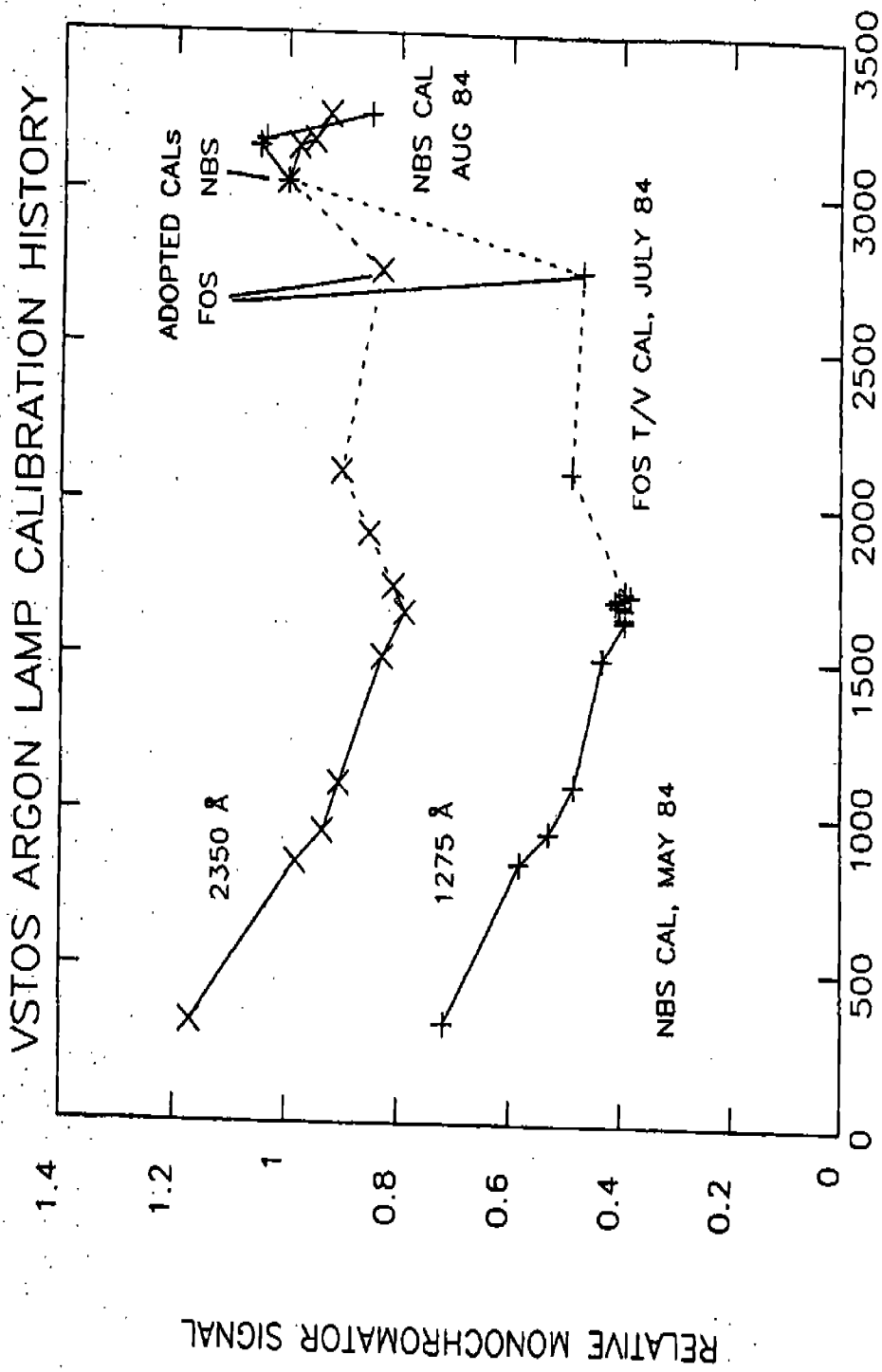


Figure 6.2.2.4.5-2. VSTOS Argon Lamp Calibration History

ment. No correlation with chamber pressure is obvious; e.g., the chamber was opened (to insert the diffuser on Pt-Cr-Ne lamp #1) and reevacuated in the middle of the first NBS run, but the fluxes do not mirror the resulting changes in operating chamber pressure.

The Pt-Cr Ne lamps each suffered drops in the measured line fluxes from the May to August calibrations, with an average decrease of ~10% for the #1 lamp and ~23% for the #2 lamp. No correlation with wavelength is apparent. This is consistent with the variations seen during life tests performed on an identical lamp at the Johns Hopkins University in 1981, which showed flux changes as great as a factor 2 over 1 Amp-hour of intermittent operation (at 10 mA). The 'workhorse' #2 lamp, used for alignments and many tests of the FOS other than the APC, experienced ~1.5 Amp-hours of use (or ~15% of its expected life) in the interval between the May and August calibrations, while the #1 lamp logged ~.25 Amp-hours (both also operated at 10 mA).

6.2.2.4.5.1 Uncertainties in VSTOS Calibration

In addition to the monochromator calibration uncertainties, the many sources of error described above must be accounted for in our estimates of the accuracy of the absolute VSTOS irradiance assignments. Following is an attempt to estimate these uncertainties.

1. VSTOS carousel repeatability and NBS system stability, including repeatability in positioning of the PMT. The maximum total error due to these can be estimated from the repeatability of the Pt-Cr-

Ne #2 lamp measurements which were made periodically throughout the calibrations, at less than $\pm 3\%$.

2. VSTOS/monochromator alignment. The signal of a line from the Pt-Cr-Ne #2 lamp was maximized to within an estimated $\pm 2\%$. This implies a maximum offset of less than 250 μ which, in the worst case of the krypton lamp in the NUV, would imply a signal loss of $< 6\%$ based on the image maps taken. Flux loss due to tilt misalignment, independent of which lamp is in use, is less than $\pm 2\%$.
3. Monochromator response to VSTOS beam. The correction factors derived from the monochromator mapping are subject to assumptions of uniform flux distribution over the VSTOS beam, size of the central obscuration, and (probably of greatest importance) that the response at any point is the product of the responses on the horizontal and vertical axes which intersect at the optical axis. We have no means of determining these uncertainties accurately, but estimate a maximum tolerance of $\pm 5\%$ in the correction factor.
4. Monochromator pass band. Although this was measured to within $\pm 2\%$ at 12930, it was later realized that the pass band is dependent on wavelengths, requiring a correction by 13% at the shortest wavelengths according to calculations. This was

not empirically verified, however. This is important only for the spectral line sources (Pt-Cr-Ne lamps).

5. Signal-to-noise ratio, system nonlinearity, and chart reading errors. These are generally accurate to $\pm 2\%$ with the following exceptions due to lower S/N:

- all argon lamp measurements: $\pm 5\%$
- Pt-Cr-Ne #1 $\lambda \leq 1723$: $\pm 5\%$
 $\lambda \geq 1916$: $\pm 3\%$
- Pt-Cr-Ne #2 $\lambda 1248, 1404, 1622$: $\pm 3\%$
 (small aperture/slit configuration)

6. Lamp variability. This is probably the dominant error source for each of the continuum lamps, since their behavior is not consistent through the calibration period. We defer estimation of these errors to Section 6.2.3, where they are discussed in the context of the FOS APO.

With the exception of the effects of lamp variability then, the total uncertainty in our calibration of the VSTOS may be summarized as follows: all measurements above 2000 Å are accurate to within $\pm 11\%$, degrading to $\pm 17\%$ at the shortest wavelengths, with the error in all cases being dominated by the uncertainties in the absolute calibration of the monochromator response.

6.2.3 FOS APC

6.2.3.1 General Method

Absolute photometric calibration of the FOS was performed during the June through August 1984 test periods at MMDA, by using both the ambient and vacuum STOSs as sources of known irradiance at the FOS entrance apertures. With the aperture areas known, the photon flux at each wavelength of interest entering the FOS can be calculated and the efficiency, or quantum throughput (QT), measured by comparison of these fluxes with the resulting count rates. This QT should be the product of the optical efficiencies (reflectances of the mirrors, transmittances of the filters and prism, etc.) of the components along the light path and the quantum conversion efficiency (QE) of the Digicon detector, if none of the flux entering the FOS is lost due to STOS misalignment or overfilling of the FOS optics. The geometry of the STOSs was designed to slightly underfill the FOS optics (in the same manner as the ST OTA), but losses will occur if small misalignments exist.

Some flux may also be lost due to diffraction by the smallest FOS apertures, particularly at long wavelengths. Dr. Richard Allen has made an estimate that such losses may be as large as 32% at 6000 Å through the A4 (.1⁰⁰) apertures. Preliminary results of calibration tests to determine the extent of light loss due to diffraction indicate that the wavelength dependence of the Allen estimates is correct. The actual aperture size measurements used for the APC reduction were made by integrating the flux scan through the various apertures (with the

camera mirror) and thus represent a mean effective size over the wavelength response of the detector convolved with the spectral flux distribution of the FEL lamp. For the blue side measurements, the wavelength for which the aperture size is representative is ~ 14000 ; for the red side ~ 17000 . (The latter measurements were made with the ASTOS FEL lamp current reduced to 4 Amps, causing it to be very red.) Assuming these mean wavelengths, the effective aperture areas, corrected for diffraction losses according to Allen's estimates, were used for the APC measurements made with the A4, A3, and B2 apertures. We estimate the uncertainty in the absolute aperture areas at $\pm 5\%$, with the exception of the A4 apertures: their small size, relatively ragged perimeters, and large diffraction loss corrections render these areas uncertain to $\pm 10\%$.

All calibration data was taken in the standard spectrophotometric mode, with quarter stepping and an overscan of 5 diodes. The raw data were corrected for dead time (paired pulse correction) with time constants $t_1 = -1.08(-8)s$ and $t_2 = 1.92(-8)s$, according to the relationship described by Ebbets (1985). In a few cases, this correction is large (as great as 50%), but the majority of the APC data involve observed count rates below 10,000 counts/s/diode, at which the correction is about 10%. The accuracy of the correction is estimated to be within $\pm 2\%$ for observed count rates below 10,000, escalating to $\pm 5\%$ at 30,000 and $\pm 10\%$ for the few APC data points near 33,000 counts/s/diode. These uncertainties derive from the errors inherent in the paired pulse correction calibration, which relies on accurate knowledge

of the relative aperture area. Efforts are currently being made to improve the accuracy of the count rate correction.

6.2.3.2 Ambient APC

The FOS QT was measured with the ASTOS in both June and August 1984. The alignment of the ASTOS with each side of the FOS was checked during the June calibration by successively occulting all of the beam except a small circular area at the beam edge, centered on each of the spider legs supporting the ASTOS occultation aperture disk. If the ASTOS is significantly misaligned, the resulting signal from each quadrant would be different and the sense of the misalignment could be readily deduced. The deuterium lamp was used to illuminate the A4 apertures and aperture maps were made with the camera mirror. Prior to the June APC, the ASTOS was found to be in excellent alignment on the FOS blue side, with variations among the quadrants of less than 4%. A later check, after several ASTOS repositionings and immediately following the APC measurements, yielded less desirable results, with deviations up to 9% from the mean, but nevertheless indicating relatively small beam loss. On the red side, however, the results indicated significant misalignment, the 'W' image containing only ~47% of the signal in the 'E' image, while 'N' and 'S' were essentially identical and slightly less than 'E'. The diameter of the test aperture 9.9 mm, and the ASTOS occultation aperture diameter is 33.1 mm and 14% of its area is occulted. We can infer from these data that the fraction of the ASTOS beam lost on the red side was most likely between 10 and 20%. The large uncertainty is due to effects of diffraction.

through the A4 aperture, which make the computation of beam loss unwieldy and dependent on wavelength and aperture size used, since where the diffraction losses are large, we would expect the sensitivity of misalignment to be reduced. Similar calculations for the blue APC yield a beam loss estimate of $8 \pm 2\%$.

An attempt was recently made (23 Feb 85) at LMSC to align the ASTOS on the red side with essentially the same technique, but utilizing the B9 aperture (for which diffraction losses are negligible) and the FEL lamp, operated at reduced current (4A). Considerable realignment was required to equalize the 4 quadrants. Spectra representing a subset of the standard APC procedure were obtained with the FEL lamp #179 at nominal current (8.01A). These spectra contained only ~.78 of the flux seen in the 'misaligned' August 1984 spectra, independent of wavelengths from below 3000 to above 8000 Å. Since internal calibration lamp spectra and flat-field LED exposures made subsequently produced results nearly identical with many previous tests (including those made in August 1984), the instrument has not degraded, and we can only conclude that the ASTOS alignment technique used here is faulty in some manner. The data obtained with the ASTOS in its original, nominally aligned orientation must therefore be taken, at face value, but since some beam loss which we cannot quantify may indeed be present, the efficiencies calculated from those spectra represent lower limits to the true FOS QT.

Comparisons of the raw data from the June calibration with those of the August run indicate that the FEL lamp measurements

are very repeatable. The August spectra almost all appear to have count rates that are approximately 4% ($\pm 2\%$) greater than the levels of the earlier spectra, with no obvious or systematic wavelength dependence. This is consistent with the fact that the August measurements were made with the Digicon operating voltage at the flight values: 20.9 kV (red) and 22.4 (blue), while the June data were obtained at 18.4 kV. The exceptions are both August measurements of the H57 grating on the red side which show a loss of signal at both ends of the spectrum; the spectrum taken through the B2 aperture is very clearly missing the diode array with nearly half of the light lost at each end of the spectrum and 20% lost near the central wavelength. This same effect is also present in the A4 spectrum, and is interpreted as due to improper centering of the image on the diode array caused by the nonrepeatable positioning of the filter grating wheel. The wavelength dependence is due to the 'C' distortion inherent in the Digicon. Y-scans were made before each of the June APC spectra to determine the correct Y-base (to center the spectrum on the array). We have taken the June H57 A4 spectrum and scaled it according to the ratio of the count rates at the center of the spectra from June and August (1.03) to calculate the QT for this configuration. The August data are adopted directly for all other configurations.

The GS-179 FEL lamp was used for all of the APC measurements with the exception of the August calibration of the blue side when the GS-180 lamp was employed. Both lamps were calibrated at the NBS and very little difference exists in their respective

irradiance; the GS-180 lamp is a bit hotter, but between 2600 Å and 8000 Å, the differences are less than 3%. Diffusing screen #2 was used throughout the APC. As previously mentioned, some uncertainty exists in the lamp current because of failure of the power supply, but this is minimal, affecting the irradiance by less than 2%.

The deuterium lamp measurements were much less repeatable than the FEL data and very obvious differences in both overall count rate and spectral distribution were present, especially in the blue side data. The poor quality of their calibration and this non-repeatability have rendered the deuterium lamps of little value, and we have elected not to treat these data further.

The count rates were determined generally to within $\pm 2\%$, with some degradation in accuracy due to poor S/N at the blue end of the prism spectra ($\pm 5\%$ at 12000 and $\pm 10\%$ at 12600). Because of the large integrated flux of the FEL lamps and the wide range of sensitivity of the detectors (especially broad for the 'red' Digicon), some corrections to the observed count rates for scattered light were required for measurements below 3000 Å. The contribution due to scattered light was determined in a fairly straightforward manner: a separate calibration procedure, designed to measure the light scattering properties of the FOS, was executed during the August ambient calibration period. Since this procedure made use of the ASTOS with the calibrated FEL lamps and a series of blocking filters to directly determine the amount of scattered light in both H27 and prism spectra on both

red and blue sides, we need only scale these measurements according to the relative aperture sizes used for these and the APC spectra. A small additional contribution that does not scale with aperture size and is presumably due to light from the room entering the spectrograph (at places other than the entrance aperture) and scattering directly to the detector, was measured by placing an opaque screen over the blocking filter. The resulting total correction for the H27 grating amounts to ~12% at 12500, falling to <2% at 12800, on the red side, and ~3.5% at 12500 on the blue side. The prism corrections are larger: scattered light accounts for ~21% of the observed count rate at 12600 and 4% at 13000, on the red side.

The FOS QT was calculated from:

$$\begin{aligned}
 QT &= \frac{\text{count rate per diode}}{\text{photon rate per diode}} \\
 &= (1.989 \times 10^{-7}) \left(\frac{R * (L - \text{Recat})}{E_{\lambda} * A * d_{\lambda} * a * \lambda * \Delta\lambda} \right); \quad (6.2.3.2-1)
 \end{aligned}$$

where R is the raw count rate per diode, L is the detector linearity correction (typically 1 to 1.1), Recat is the estimated count rate due to scattered light, E_{λ} is the ASTOS spectral irradiance (W/cm^2), A is the true aperture area (cm^2), d_{λ} is a correction factor for diffraction losses through the aperture (0.6 to 1.0), 'a' is the fraction of the ASTOS beam seen by the FOS as a result of ASTOS misalignment, and $\Delta\lambda$ is the FOS dispersion ($\text{\AA}/\text{diode}$) at the wavelength of the measurement, λ (\AA). Because of our inability to directly estimate the extent of ASTOS misalignment, as described above, 'a' has been set to 1 for these calcu-

lations (but see Section 6.2.5.1). The results of the ambient APC measurements are displayed in Figures 6.2.3.2-1 and 6.2.3.2-2 for the red side and 6.2.3.2-3 and 6.2.3.2-4 for the blue side. Error bars reflect the uncertainties discussed above. Since the ASTOS deuterium lamps proved useless and the FEL lamps were calibrated only above 2500 \AA , no measurements of the H19 or L15 gratings were obtained with the ASTOS.

6.2.3.3 Vacuum APC

The FOS QT was measured with the VSTOS, on the blue side only, during the July 1984 thermal vacuum testing at MMDA. Three separate measurements were made, but because of a VSTOS misalignment problem only the last of these, on July 22, is useful for direct QT determination. After the second measurement, mapping of the VSTOS image by single-stepping its lamp carousel showed that the image centers were about one carousel step CCW of the nominal position at which APC data was previously obtained. This is believed to be due to misphasing of the carousel and motor when the VSTOS was mounted and realigned with the FOS in the vacuum chamber. (A prior, careful alignment was lost when the adjustment shims were accidentally misplaced.) The final set of APC measurements was therefore obtained with the carousel always positioned one step CCW of the nominal. The image maps made during the APC, when compared with those obtained when the VSTOS was recalibrated in August, indicate that at this new position the VSTOS was fairly well aligned, so additional corrections for misalignment will be small.

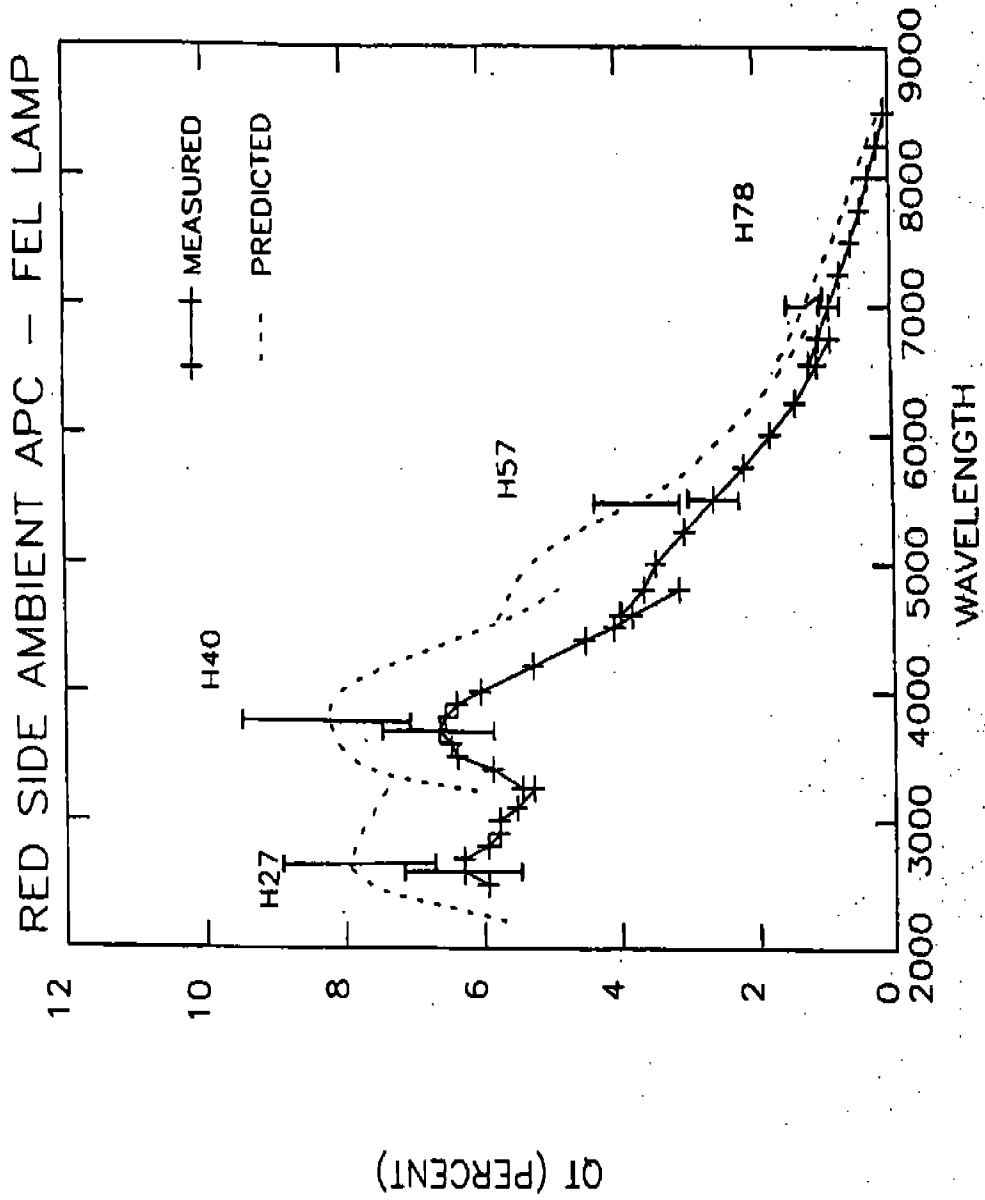


Figure 6.2.3.2-1. Ambient APC - Red Side High Resolution Gratings.

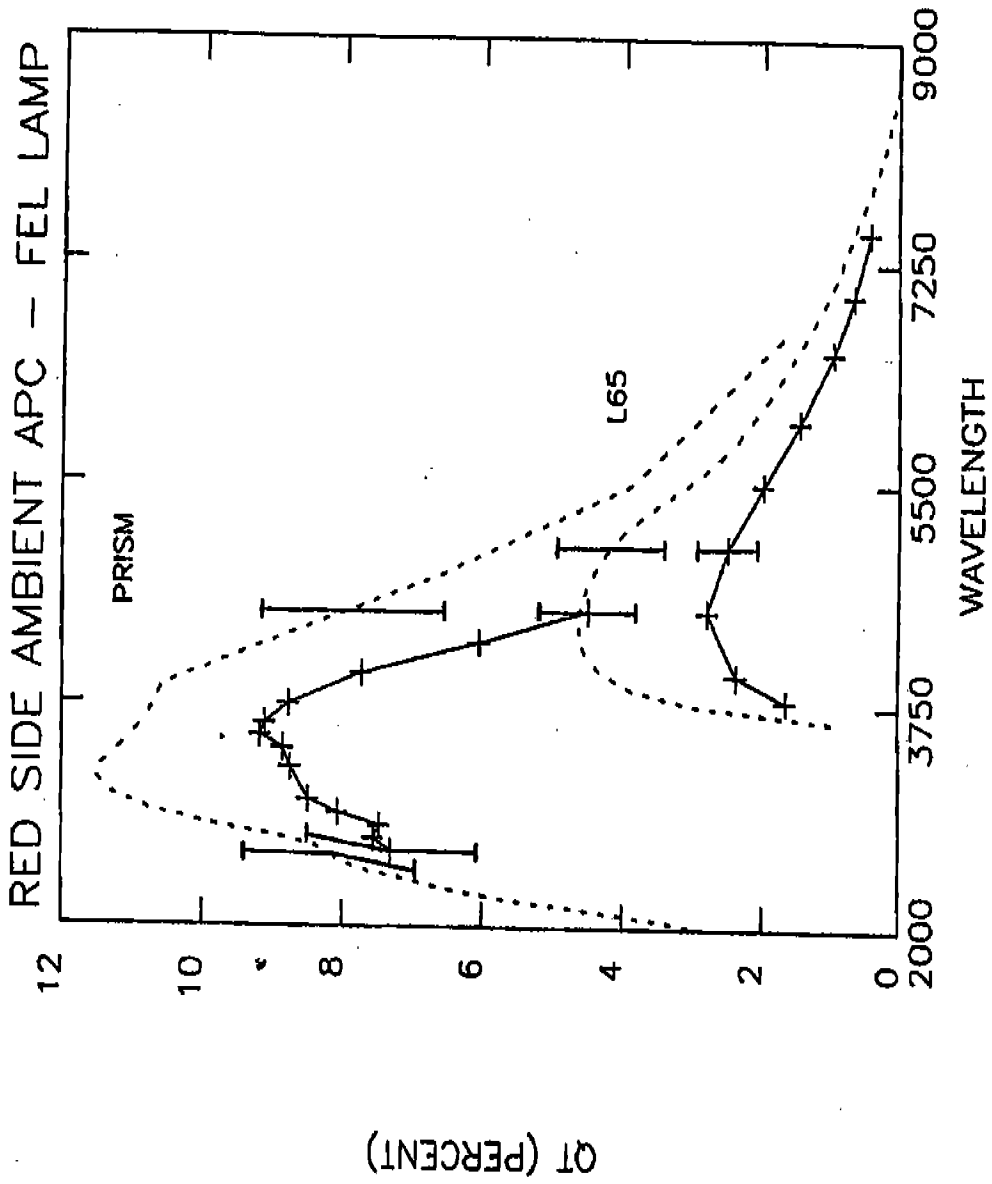


Figure 6.2.3.2-2. Ambient APC - Red Side Low Resolution Dispersers

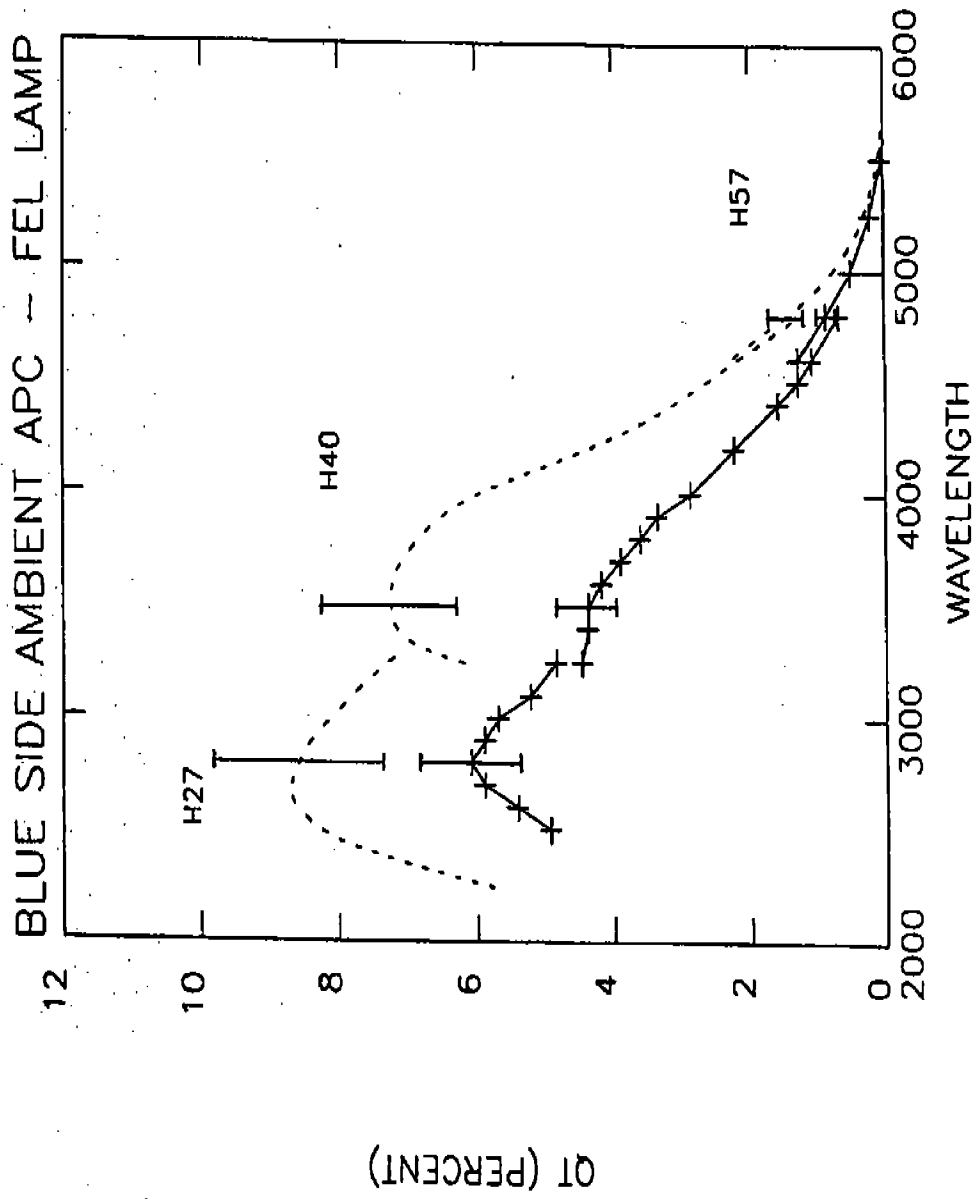


Figure 6.2.3.2-3. Ambient APC - Blue Side High Resolution Gratings

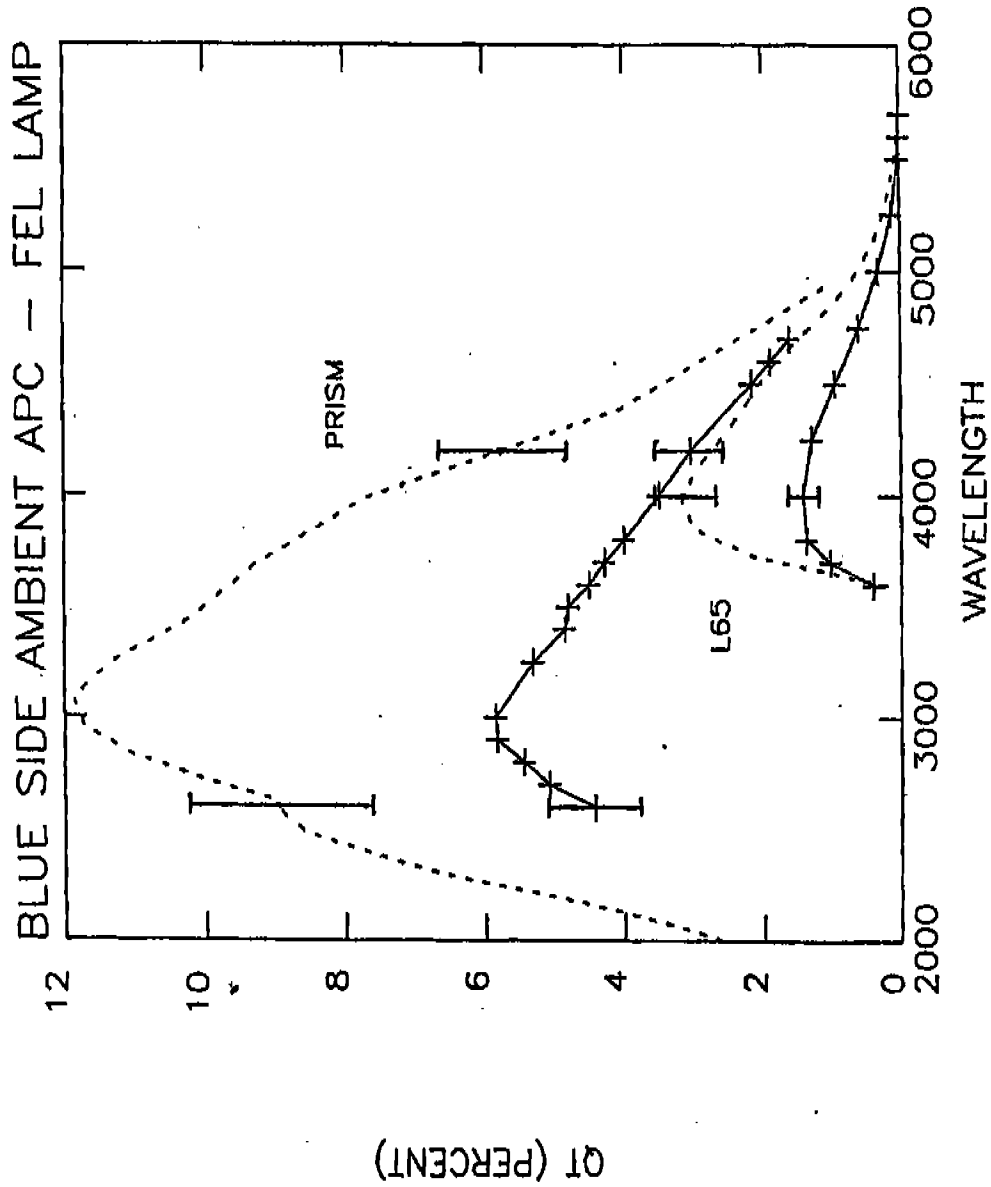


Figure 6.2.3.2-4. Ambient APC - Blue Side Low Resolution

The Pt-Cr-Ne #2 lamp is very sensitive to image misalignment, so we have inspected the image maps, made with the A3 aperture pair, to estimate how well the VSTOS images were centered on the FOS apertures; at the one step CCW position, the upper aperture spectrum was about 9% brighter than the lower. Since the upper aperture has been measured to have ~2% greater area, the misalignment in the direction perpendicular to dispersion is responsible for ~7% less flux in the lower aperture. The lower apertures are used for all of the APC spectra. The April VSTOS image mappings of this lamp can be used to infer in a self-consistent manner that ~600 μ of residual image displacement was present, nearly all in the 'Y' (perpendicular to dispersion) direction. Since the VSTOS was calibrated with the signal from this lamp maximized, the (lower aperture) APC data should be corrected for the ~7% light loss. The diffused Pt-Cr-Ne #1 lamp is very insensitive to image misalignment, so no correction is required in this case.

Since similar mapping data, in both upper and lower apertures, is not available for the other lamps, it is difficult to make accurate misalignment corrections for these, especially since the image size and shape was found to have strong wavelength dependence for the argon and krypton lamps, and the argon and hydrogen lamp profiles are asymmetric. The following estimates of these corrections (fraction of calibrated VSTOS flux seen by the FOS) are based on interpolation of the (coarse) maps made at the NBS in August, assuming a 600 μ displacement as suggested above:

Krypton lamp	NUV (λ 2400):	.85
	FUV (λ 1440):	1.10
Argon lamp	NUV (λ 2300):	.79
	FUV (λ 1280):	.87
Hydrogen lamp	λ independent:	1.06

The argon lamp corrections include adjustments based on the ratio of the signals measured at the nominal and one-step-CCW positions, since we are obliged to use APC spectra taken at the former carousel position, because argon spectra were omitted from the July 22 recalibration due to lack of time.

The above discussion deals only with misalignment of the VSTOS image with the FOS apertures; since the VSTOS produces an f/24 beam to nearly fill the FOS collimator, the APC measurements are also sensitive to VSTOS tilt. The original tilt adjustment was performed by placing a cover over the collimator which masked all but a small area (a series of small holes) along one edge and adjusting the VSTOS tilt until the signal from each of four orientations of the cover (rotated in 90 increments) were about equal. The necessity of moving the carousel one stop CCW from its nominal position to recenter the images implies some amount of tilt misalignment. This is probably small; the fraction of the (centrally-obscured) beam loss due to the tilt caused by one carousel step, if the collimator is just filled, is about 6%. The collimator is nominally slightly underfilled and diffraction through the smallest apertures will cause an overfilling which reduces sensitivity to tilt, but the intermediate case of a small amount of diffraction (e.g., through the A3 aperture) may cause

beam loss due to tilt to approach 6%. Because of the intractable nature of this calculation and uncertainties in the tilt misalignment (with the carousel in its nominal position) produced when the VSTOS was realigned, we will not attempt to apply a correction to the APC data.

The high degree of variability of the VSTOS continuum lamps was discussed in Section 6.2.2.4.5 with regard to the VSTOS calibration. It was noted there that the non-systematic behavior of these lamps over the May-August interval precluded attempts to correct for the variability by simple interpolation of the NBS and FOS measurements. In order to minimize the effects of lamp fluctuations, the July 22 APC measurements and the August 7-8 VSTOS calibration were adopted for purposes of determining the FOS QT. The krypton, hydrogen, and Pt-Cr-Ne #1 lamps were essentially unused in the interval between these measurements and the #2 hollow cathode lamp was on for only several hours (for alignment of the VSTOS with the NBS system). In general, the earliest NBS scans were used, with exception of the hydrogen lamp, which operated at an anomalously low level on August 7 and the Pt-Cr-Ne #2 lamp, since the higher resolution measurements with the small entrance aperture on the monochromator, made on August 8, were desired. This policy was dictated by the general degradation in the output of the argon and krypton lamps with accumulated operating time which is evident in both NBS calibration periods and the (much slower but unpredictable) fluctuation of the hollow cathode lamp line fluxes.

An estimate of the uncertainty in the QT due to lamp variability may be made by examining the spread in count rates for each of the FOS APC measurements of similar configurations. These measurements are not indicative of the variations produced by the lamps alone, since various corrections must be applied that are somewhat uncertain in themselves, for different Digicon operating voltage and aperture size and misalignment. Nevertheless, it is apparent that the argon and krypton lamps did not degrade consistently with use during the T/V 3 calibration, as they did during each NBS/VSTOS calibration. Figures 6.2.2.4.5-1 and 6.2.2.4.5-2 show, in addition to the VSTOS calibration points, the relative signal at each FOS APC measurement, normalized to indicate the NBS system signal required if the FOS QT were just that predicted on the basis of the individual component efficiencies. The relative consistency of these data suggest that whatever mechanism is responsible for the degradation during the NBS runs is peculiar to those measurements and further recommends the policy of selecting the earliest possible VSTOS calibration data following the FOS APC.

As noted in Section 6.2.2.4.5, the August calibration of the argon lamp at short wavelengths showed a factor 2.4 increase over the May measurements. This jump and the rapid, erratic changes recorded during the August run make the FUV argon calibration highly uncertain, and we have chosen not to include these data in our estimates of the FOS QT. We estimate that in the NUV, however, fluctuations in the argon lamp output will contribute $\pm 5\%$ to the QT uncertainty, so these data are quite useful.

FOS count rate variations of $\pm 7\%$ were recorded for the krypton lamp at long wavelengths (H27), and only $\pm 2\%$ in the FUV (H13). The latter is probably an overly optimistic indication of the variability (only three measurements were made); we adopt $\pm 5\%$ as more representative.

The hydrogen lamp continued to vary unpredictably through the FOS calibration, with variations of $\pm 10\%$ for the vacuum measurements. Both measurements made during the ambient APCs showed an apparent decrease in the hydrogen lamp flux by nearly a factor of two; these are clearly inaccurate indications of the FOS QT and may be due to differing operating characteristics of the lamp, depending on whether it is used in vacuum or at ambient.

The Pt-Cr Ne lamps both show a general trend toward decreasing line flux with usage, although this is not uniform and varies from line to line. As an example, the #2 lamp output from the 12930 line decreased by $\sim 7\%$ from July 22 to August 28, while the 12733 line remained constant and 12487 increased by 20%. This lamp logged approximately 17 hours of operation between these measurements, while only 4 hours of use elapsed between the adopted FOS APC and NBS calibration on August 8. We estimate the uncertainty in the QT due to fluctuations in these lamps at $\pm 5\%$.

The FOS QT was calculated from the continuum source measurements, in the same manner as for the ASTOS APC, so Equation 6.2.3.2-1) applies, except that the VSTOS irradiances have been calculated in $\text{mW}/\text{cm}^2\text{nm}$ (instead of W/cm^2) requiring that the conversion constant be changed to 1.989×10^{-9} . No scattered light

corrections were required for the vacuum APC spectra. The line source measurements are reduced with:

$$QT = \frac{\text{count rate in line}}{\text{photon rate in line}} = (1.989 \times 10^{-9}) \left(\frac{\int \Delta\lambda (R * L)}{E_{\text{line}} * A * d_{\lambda} * a * \lambda} \right) \quad (6.2.3.3-1)$$

where E_{line} is the line irradiance in $\mu\text{W}/\text{cm}^2$ and the other quantities are as defined for Equation (6.2.3.2-1). Since the FOS resolution is generally much higher than that of the NBS monochromator and the spectral lines are not well isolated in many cases, the FOS count rates are summed over the bandpass used for the NBS measurements. Since the NBS resolution exceeds that of the FOS prism for $\lambda > \sim 2500 \text{ \AA}$, some correction to the long wavelength line rates was required. This was estimated by taking the ratio of the flux in the NBS bandpass to that within the FOS prism bandpass (centered on the line wavelengths) in the Pt-Cr-Ne #1 H27 spectrum and applying this factor to the prism data. The corrections were 20% or less, and we estimate that their contribution to the QT uncertainties is minor. Because of the excessive blending of the 11622, 11670, 12269, and 12357 lines, combined with the small but non-negligible wavelength uncertainty for both the NBS and FOS calibration spectra (especially for L15 and the prism), the estimated errors in the QT determined at these wavelengths are somewhat greater than for the better-separated lines.

The results of the vacuum APC of the FOS blue side are shown in Figures 6.2.3.3-1 through 6.2.3.3-4. Error bars reflect the uncertainties discussed above.

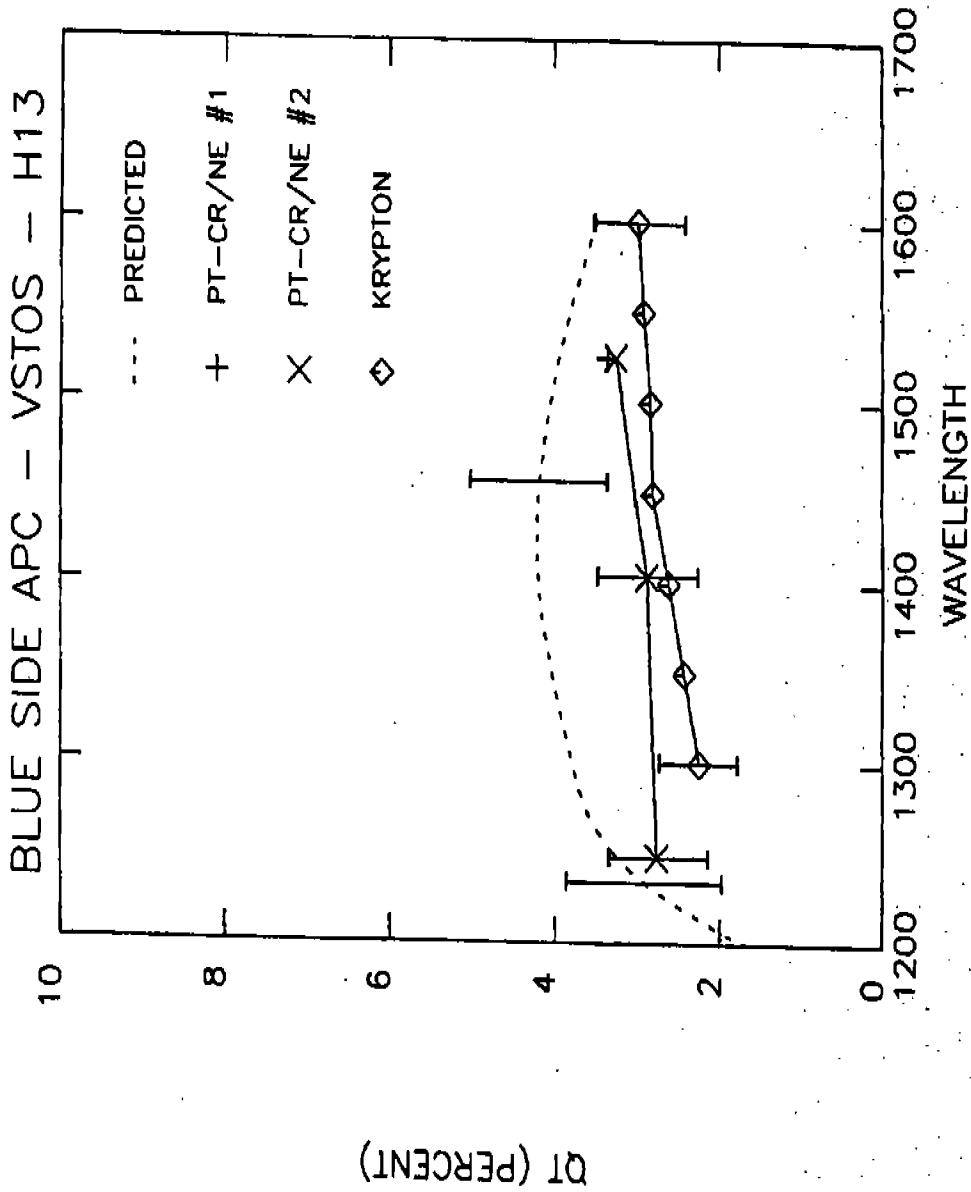


Figure 6.2.3.3-1. Vacuum APC - Blue Side G130H

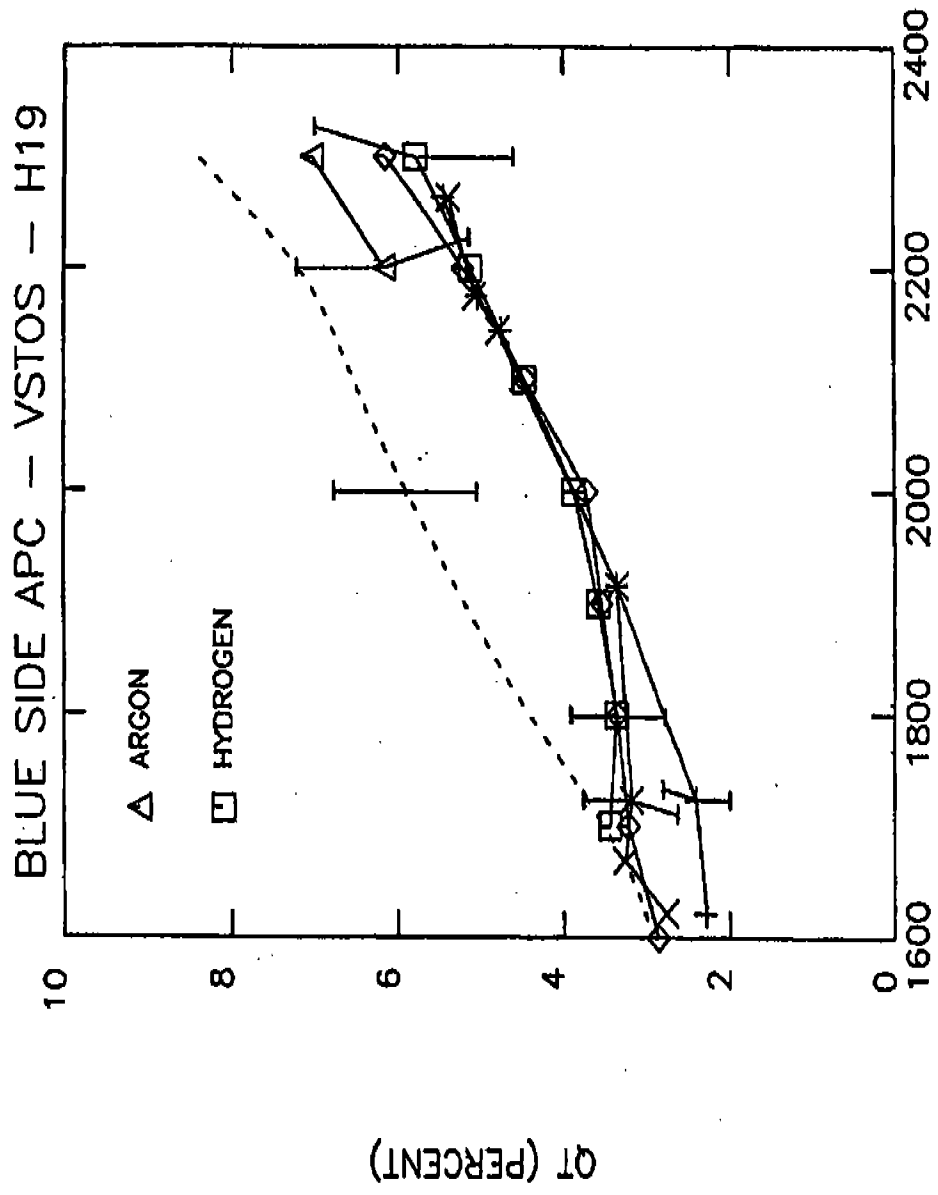


Figure 6.2.3.3-2. Vacuum APC - Blue Side G190H

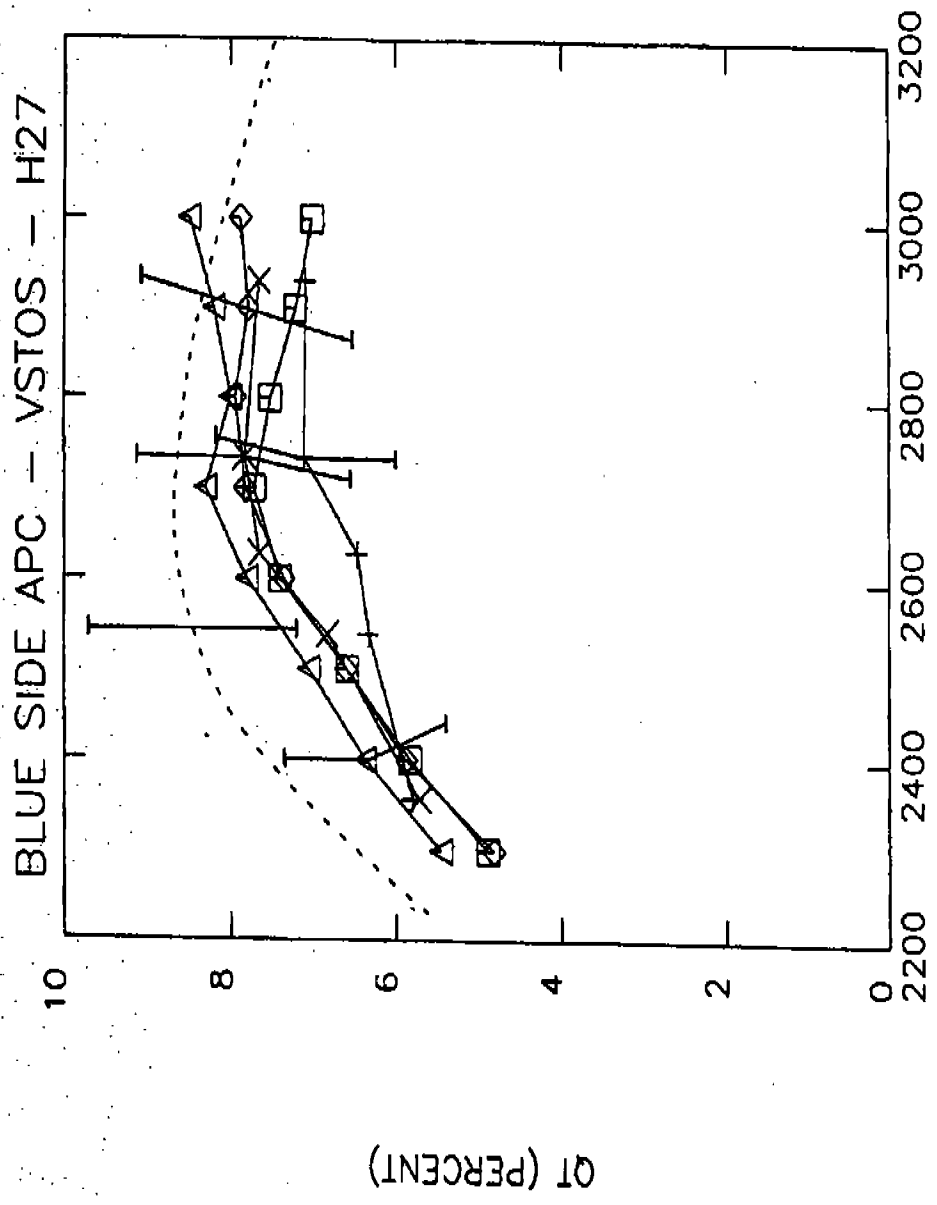


Figure 6.2.3.3-3. Vacuum APC - Blue Side G270H

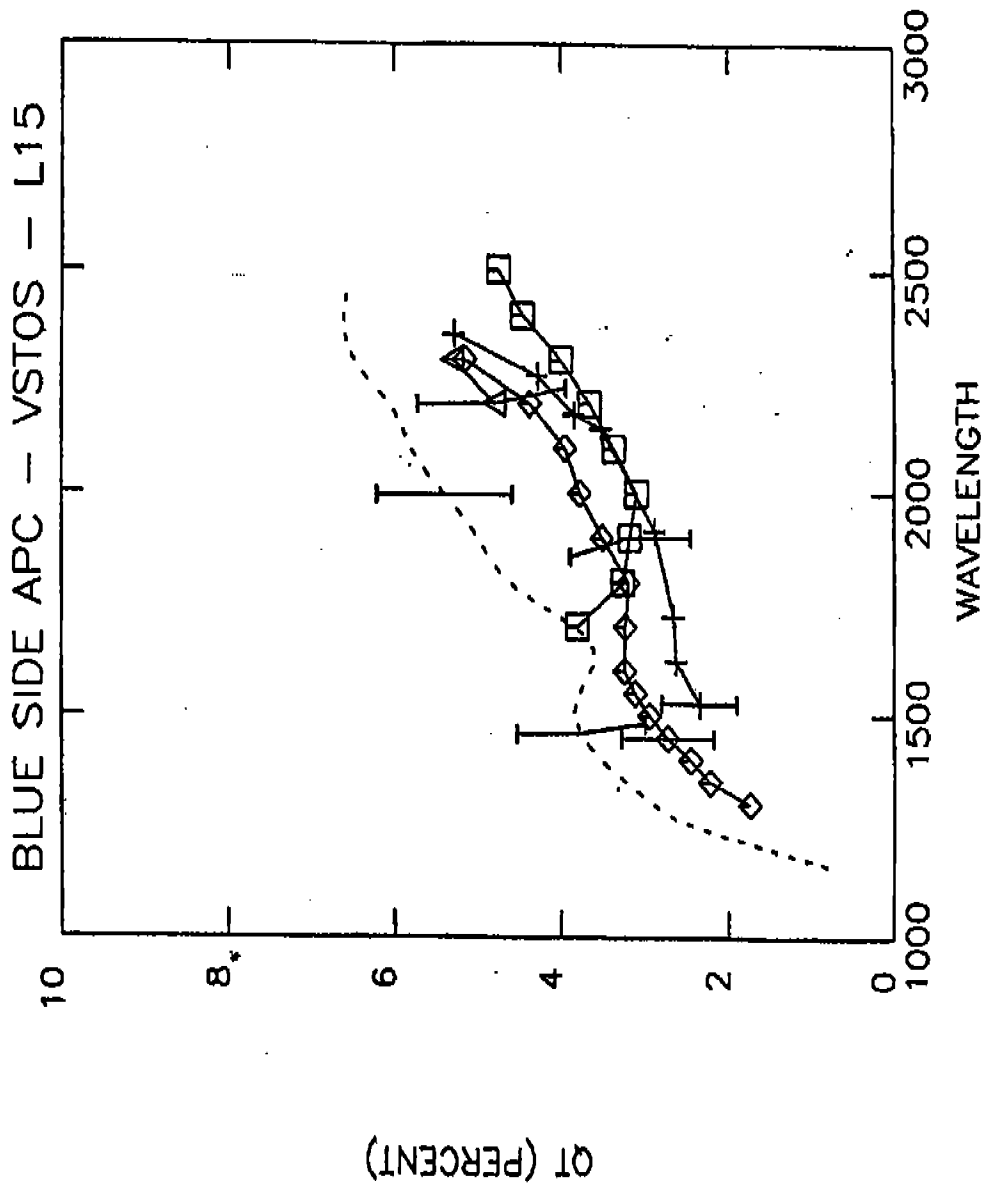


Figure 6.2.3.3-4. Vacuum APC - Blue Side G160L

6.2.4 FOS Component Calibrations

Each of the FOS optical components, gratings, mirrors, filters, and prism were measured at the Johns Hopkins University (JHU) Physics Department to verify their performance and allow selection of the elements to be used in the flight instrument. The quantum efficiency of the Digicon detectors was determined by their manufacturer, EVSD, for the same purposes. We can employ these measurements of the selected components to determine the expected overall FOS efficiencies. It is the purpose of this section to present the predicted efficiency data, with estimates of their uncertainties, so that these can be compared with the end-to-end measurements previously discussed. Details of the individual component measurements are beyond the scope of this report.

6.2.4.1 Optical Components

The JHU optical component measurements employed several separate facilities. Two comparators, one for measurements above 3000 Å and one for the UV ($1150 \text{ \AA} < \lambda < 3100 \text{ \AA}$), were configured to illuminate the dispersers with collimated light at the proper angle of incidence. These utilized PMT detectors on translating stages preceded by exit slits at the proper distance from the comparison and test mirrors and gratings, and faithfully reproduced the optical configuration of the FOS. The comparators were preceded by 1/2 m scanning Ebert monochromators, illuminated by hollow cathode lamps (Pt-Cr-Ne and Cr-Ne were used in the visible and Pt-Ne in the UV). Transfer optics and apertures were used to produce a beam that uniformly illuminated the test piece such

that it is just underfilled, again simulating the FOS conditions. Plane polarizers, a polymer film type for the visible, and one employing a single Brewster's angle reflection off bare LiF for the UV, were also incorporated in order to measure the optical efficiency for light polarized in the planes perpendicular and parallel to the grating rulings. The comparators allowed the direct cross-calibration of a test mirror or grating with a reference mirror of the same dimension and focal length, which results in very small errors, because the beam path is identical for both pieces.

The reference mirrors were evaluated in separate facilities for UV and visible reflectivity measurement, each carefully configured to minimize errors due to beam size and nonuniformity, PMT photocathode nonuniformity and sensitivity to orientation, as well as source variations. Different configurations were employed for each mirror type: plane, grazing incidence, collimators (1 m focal length), camera, and spherical (1/2 m focal length).

For all of the measurements, analog PMT currents were recorded on calibrated chart recorders and these data were manually reduced. The measurements were performed chiefly by Mr. Charles Bowers under the direction of Dr. George Hartig, and the data were reduced by Mr. Richard Pembroke. Comments on the calibration of each component type, with estimates of their uncertainties, follow:

6.2.4.1.1 Concave Reference Mirrors

The UV and visible reflectivity measurements, each made with

entirely distinct apparatus in different configurations, agree quite well at their juncture near 3100 \AA (although little or no overlaps in the wavelength coverage exists). For the collimators, the agreement is within 2%. A rise of ~5% occurs from the UV to visible reflectances of the spherical mirrors, but this may be due, at least in part, to a real feature in the reflectance curve. The measured reflectance curves are also in agreement with that calculated from the optical constants, assuming a 250 \AA MgF_2 coating on Al; the measured values lie typically ~5% below theoretical and show a departure from this trend only in the vicinity of 1650 \AA where an anomalous dip in reflectance is known to occur for these coatings. We estimate that the absolute reflectivities of these mirrors, against which all the other mirrors and gratings have been evaluated, is determined to within $\pm 5\%$ of their true values, over the entire wavelength range of the measurements.

6.2.4.1.2 Collimators

These were, in general, calibrated by comparison with the UV and visible reference collimators. The statistical errors incurred by this comparison are small, estimated at $\leq 2\%$, except at 1199 \AA ($\pm 8\%$) and 7943 \AA ($\pm 7\%$). The measurement uncertainty is therefore essentially that of the reference mirror. An exception is the red side collimator, which was used as the visible reference mirror and as such was directly calibrated.

6.2.4.1.3 Gratings

The gratings were measured by comparison with the UV and visible spherical reference mirrors. Care was taken to assure

that the proper angles of incidence and diffraction were used; alignment was performed by measuring the zeroth-order reflection geometry with the aid of a laser. In addition to the overall, first-order reflectance (with the grating nearly filled), the efficiency of each panel of the (multipartite) gratings was measured, with a stopped-down beam. Although no central obscuration (as present in the actual FOS beam) was utilized in the full-illumination measurements, the resulting 'error' is negligible, since the efficiency of each panel does not deviate strongly from the mean. The H13 and H19 gratings were replaced in the FOS and their spares remeasured before mounting; the measurements are in excellent agreement (<2%) at points near the center of their wavelength coverage ($\lambda \approx 0$), but some significant disagreement is present at the wavelength extremes, especially for H13 at points below 1248 Å. The latter may be due to some real degradation, amounting to ~15% at 11219, presumably due to surface contaminants, despite the care taken in grating handling and the fact that the gratings were stored in their special, O-ring sealed containers in the intervening two years. The other discrepancies may be at least partly due to slightly different grating alignments, with corresponding shifts of the blaze wavelength, which would be most apparent at the larger diffraction angles, where the efficiency falls rapidly as λ departs from the blaze.

6.2.4.1.4 Prism

This was measured as an assembly after the prism was bonded to the spherical mirror and was treated in the same manner as the

gratings. Again, the agreement between UV and visible measurements is good (0.81 at 3065 Å with the UV monochromator, and 0.805 at 3323 Å with the visible). Reasonable agreement with the measurements was obtained by an attempt to calculate the efficiency using the optical constants of the MgF₂ A/R coating and sapphire, although some variance exists in the published data (Pembroke, 1983).

6.2.4.1.5 Grazing Incidence Mirrors

These were measured directly (not with respect to a reference mirror), although for the visible measurements use was made of a pair of auxiliary flats and a beam-splitter in a double-pass arrangement that permitted the single PMT to remain stationary. One flat returned the beam reflected by the grazing mirror and the other reflected the beam when the grazing mirror was removed; both were used at normal incidence. Because the beam made two reflections at the proper angle of incidence (76.5 degrees, chief ray), the accuracy is improved. However, we note that although care was taken to illuminate approximately the same area of the mirror as is used in the FOS, a central obscuration was not present and the ±1.2 degree range in angle of incidence presented by the OTA f/24 beam was also not exactly duplicated, since the test beam was nearly collimated. Nevertheless, we expect that these differences incur only very minor errors. The UV measurements were made in a direct fashion, and excellent (<2%) agreement between these and the visible reflectance near 3000 Å was again achieved. Each face (red side and blue side) was measured. Separate measurements were made with plane polarized light in

directions perpendicular and parallel to the plane of incidence, showing the expected substantial polarization, especially in the red. These results were compared to reflectances calculated from the optical constants for Al and Al_2O_3 , assuming a 45 \AA thick growth of the latter on the 'aged' bare Al coating (Pembroke, 1984).

6.2.4.1.6 Filters

The order blocking filters were measured at JHU only in the UV ($\lambda < 3000 \text{ \AA}$). With exception of the filter used for the H27 grating (MgF_2 coated fused silica), the measurements lie below the nominal filter cut-off and provide determinations of the amount of filter leak. Transmission measurements of the A/R coated colored glass filters provided by Acton Research Corp. (ARC, the coating vendor) were made at very high S/N and variations among pieces of the same type are very small. The ARC data for the H27 filter is in excellent agreement (within 1%) with the JHU measurements, providing confidence in both sets of data.

6.2.4.2 Digicon Q.E.

The efficiency of the flight detectors has been determined at EVSD (Division of SAI), where the tubes were constructed. A fairly comprehensive summary of the test results for each of the FOS program Digicons, including the F-8 (red) and F-7 (blue) flight-selected tubes, has been previously prepared (Beaver and Harms, 1984).

Briefly, the QEs were determined by comparison with a pair of standard photodiodes, the absolute efficiencies of which were provided by their vendors (EMR and EMI). The comparison is

generally indirect for the visible measurements; an intermediate standard Digicon was first calibrated in current mode versus the photodiode, then in turn used to calibrate the tube under test in either current or photon-counting mode. Two sets of apparatus are used to measure the UV and visible portions of the spectrum, with substantial overlap in their respective coverages. The visible standard is an EMI 9715 QAM vacuum photodiode and an EMR 549-09-00 photodiode, whose calibration is traceable to the NBS, is used in the UV. The UV apparatus makes use of a secondary standard, a PMT sensitive to visible light, to monitor the brightness of a phosphor screen, which can be moved into the beam behind the monochromator exit slit, to normalize the beam fluxes between comparison measurements of the photodiode and test Digicon. Four lamps are used for the UV measurements: Xonics hydrogen (λ 1216), Xonics krypton (λ 1236, 1460), Scientific International xenon (λ 1473) and a mercury pen-ray (λ 1850, 2537, 3131, 3650, and 4047). In addition to the current mode QE measurements made at each of these wavelengths, a photon counting mode determination was also made at λ 1216, 1850, and 2537. The agreement between the QE determined in each mode for the F-7 digicon is quite good (<5%).

The only UV QE measurements that are available for the flight detectors were made at the time of delivery in April 1981 (red) and July 1981 (blue). Subsequent tests have been made with the visible apparatus ($\lambda > 3600 \text{ \AA}$), however. For the blue F-7 tube, the measurement in April 1984 is generally in good agreement with the delivery values, but with some degradation of the

red response indicated. The red F-7 tube data are not so easily interpreted: discrepancies ranging from a factor of 1.5 to 2.0 occur in the remeasurements of July 1983 and March 1984. These lie above and below the delivery values, respectively. We suspect that a large part of the discrepancy may be due to the particularly high ion count rate exhibited by this tube, which produces an apparent enhancement of the efficiency near the tube center when the photocathode is illuminated over a wide area. This effect was as large as 50% in the most recent measurements and was accounted for by measuring the QE away from the center. The anomalously large QEs reported in July 1983 may be at least partially the result of this ion count enhancement, although the ion count rate was measured to be substantially smaller at that time. Since no recent measurements have been made below 3600 Å, we assume that the approximately wavelength independent ratio of the March 1984 to delivery values (~0.8) is valid at shorter wavelengths and derate the UV QE measurements accordingly. The 1984 remeasurements of both tubes were made with respect to the F-2 Digicon, which was calibrated (in current mode) against the EMI photodiode at the same time. These data should therefore provide an excellent cross-calibration of the two flight detectors even if systematic errors, such as degradation of the reference photodiode QEs, are present. EVSD has recently obtained another calibrated EMI (visible) photodiode and has found that the older standard has not degraded significantly.

A systematic error in the EVSD QE measurements at the shortest wavelengths was recently discovered as a result of com-

paring efficiencies measured by both EVSD and the NBS for several different detectors. The EVSD evaluation of standard photodiodes, which it manufactures for the NBS, has produced consistently higher QE than the subsequent calibration at the NBS. This discrepancy amounts to ~30% at 1236 Å, dropping to ~9% at 1460 Å and <2% for $\lambda > 2000$ Å. The HRS Digicons were also measured at the NBS, GSFC, and EVSD; for the CsTe tubes, the discrepancy is much the same, with NBS and GSFC evaluations in good agreement. The HRS CsI Digicons do not show such a marked discrepancy, however.

The EVSD UV standard photodiode has just been recalibrated (January 1988) and shows only an ~3% degradation in its QE at 1216 Å from its 1978 value; furthermore, mapping of the diode photocathode area indicated that spatial variations in its response are fairly small, so beam 'footprint' considerations are probably not the major cause of the EVSD/NBS discrepancies. The problem is most likely caused by scattering of long wavelengths, since the sources in question produce significant fluxes in the NUV. This explanation finds support in the EVSD measurements of the HRS CsI Digicons, which have a very restricted range of sensitivity (essentially blind to the NUV) and are therefore less susceptible to QE measurement errors as a result of scattered light, were in considerably better agreement with the NBS data. We have derated the EVSD measurements below 2000 Å according to the average ratio of NBS to EVSD QEs of three photodiodes which were recently measured.

An estimation of the uncertainties in the EVSD measurements can be made by inspection of the QE history of the F-2 tube, for which seven sets of data are reported in the report by Beaver and Harne (1984). The spread in these measurements, which do not exhibit a clear temporal trend (except for the original delivery data of 1981 which show a more sensitive red response), is about $\pm 10\%$ at 4000 \AA degrading to $\pm 30\%$ at 8000 \AA . Although similar data are not available for the UV measurements, we estimate the uncertainties at $\pm 30\%$ at $\lambda 1216$, where the signal-to-noise ratio is poor and corrections of that order have been applied, improving to $\pm 10\%$ at $\lambda 2537$, since the UV and visible measurements, involving entirely separate apparatus, generally agree to within 10% where they overlap.

6.2.4.3 Predicted FOS QT

The expected efficiency of each FOS observing configuration is the product of the reflectivities of the grazing mirror, collimator, and disperser, the filter transmittance (if a filter is present), and the Digicon QE, assuming proper alignment of these components and the absence of beam occultation (e.g., by misplaced baffles). The predicted QT values have been calculated, based on the measurement described above, and are shown in a set of 9 plots (Figures 6.2.3.2-1 through 6.2.3.2-4, 6.2.3.3-1 through 6.2.3.3-4, and 6.2.4.3-1), as dashed curves. The error bars represent the uncertainties in the individual component measurements, added in quadrature.

Cubic spline fits to the efficiency data were manually adjusted to remove the amplification of measurement statistical

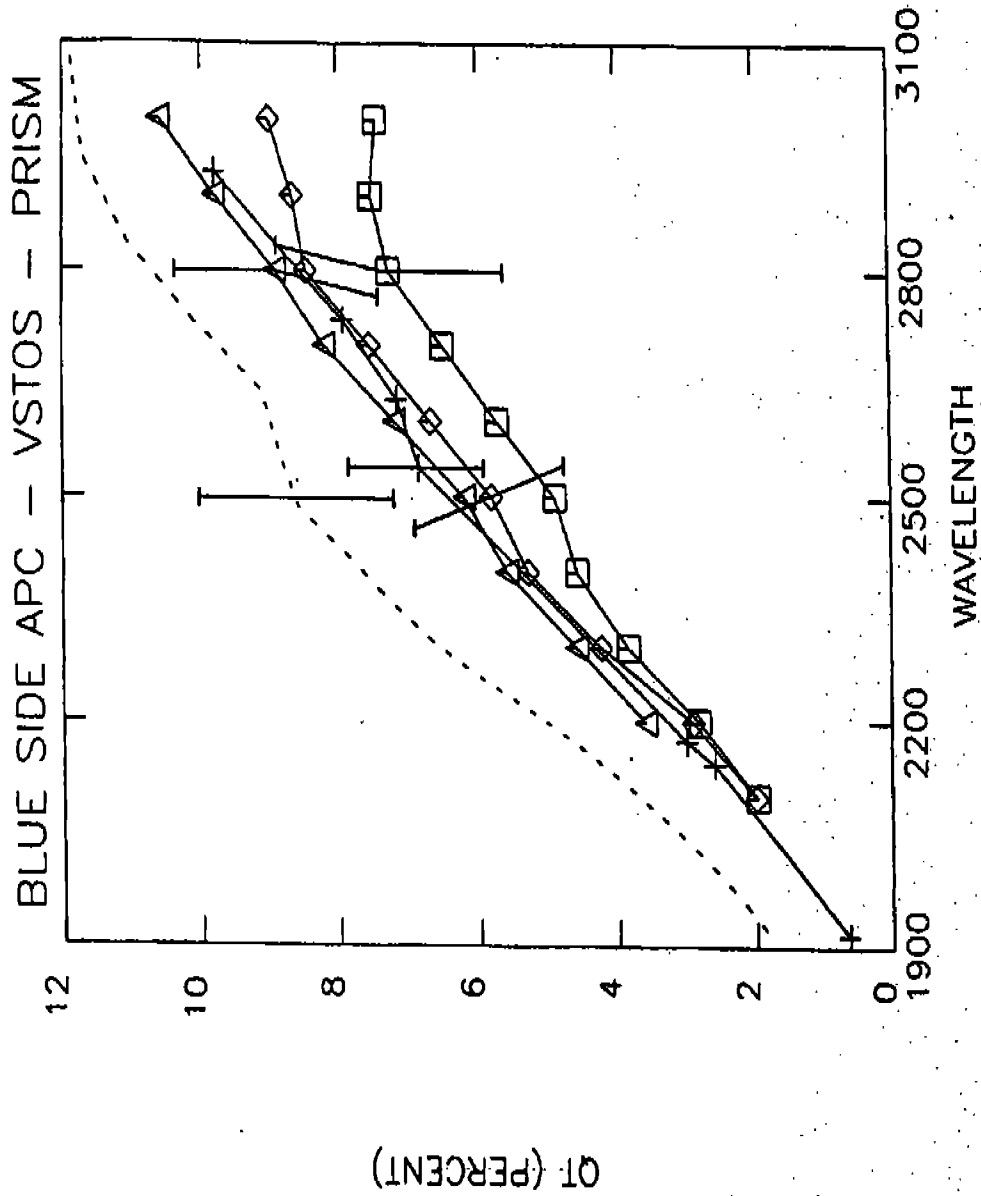


Figure 6.2.4.3-1. Vacuum APC - Blue Side Prism

error that is typical of this type of fit and to produce reasonable extrapolation of the data where required. We note that, particularly for the Digicon QE in the UV, this is a somewhat arbitrary process, since this region is poorly sampled and no recent measurements are available, resulting in a reduction in the level of confidence for the FUV efficiency predictions on the blue side, in particular.

6.2.6 Analysis and Conclusions

6.2.5.1 Intercomparison of Results: General

We can exploit the partial redundancy of many of the APC measurements to gain further insight concerning the systematic errors that may be present, thereby permitting a better estimate of the true FOS QT. An obvious starting point is comparison of H27 and prism QTe on the blue side, which were measured with both the ambient and vacuum STOS. We find that the VSTOS measurements lie, on the average, ~30% above the ASTOS-produced QTs. This is contrary to expectation that the VSTOS, which produces a rather small image at the FOS apertures, would be more difficult to align than the ASTOS, and therefore be more susceptible to beam loss due to residual misalignment (see also the discussion of VSTOS alignment problems, Section 6.2.3.3). Nevertheless, the apparently straightforward ASTOS alignment check method has recently proven doubtful as a result of an attempt to align the ASTOS with the FOS red side that resulted in 22% less measured flux than in the 'misaligned' condition (see Section 6.2.3.2). It seems reasonable to assume that losses of the same order may well be present in the nominally aligned blue side ASTOS spectra.

We may also compare the blue side ASTOS measurements of H27, H40, H57, L65, and the prism with those on the red side. As noted in Section 6.2.4.2, the blue and red detectors were measured in the visible region against the same transfer standard Digicon within a short period of time and as such should be well calibrated with respect to one another. The blue and red collimators were cross-calibrated (since the red side collimator was used as the reference mirror for those measurements) and each side of the grazing mirror, although separately measured, can be assumed to be well known, with respect to the other, since the measurements were made in exactly the same manner (and little difference in reflectivity was seen, as expected). Except for possible misalignments of the ASTOS or the FOS components, or beam vignetting by improperly placed baffles, etc., the APC measurements for each disperser should be nearly identical, with respect to the predicted QTs. Rather, we find that the red side QTs more closely approximate the predicted values, again possibly indicating blue side ASTOS misalignment losses of ~20% if the red side were perfectly aligned, and even greater losses if some red side misalignment was also present.

The majority of the discrepancy between the predicted and ASTOS-measured QTs, is most likely due to some form of misalignment or beam vignetting, since the ratio of measured to predicted efficiencies shows little global wavelength dependence, although this ratio does vary slightly over the wavelength range covered by some of the dispersers. It seems eminently reasonable, then, to normalize the blue ASTOS measurements to the VSTOS data for

H27 and the prism in order to make our best estimate of the true FOS efficiencies. The alternative is to discount the quality of the NBS VSTOS calibration at the long wavelengths, where it is most accurate. We also note that, at the wavelengths in question, the VSTOS irradiance calibration is tied most firmly (although by several intermediate standards) to the same standard used for the ASTOS calibration, since the argon mini-arc was calibrated against an FEL lamp irradiance standard with FASCAL pedigree, in the NUV. The relatively good agreement (well within the errors expected from lamp fluctuations) demonstrated by the measurements with each lamp -- representing a variety of count rates, utilizing several different entrance apertures, and including both line and continuum spectra -- lends further credence to the VSTOS H27 and prism results. Because the VSTOS was aligned with the NBS monochromator by maximizing the signal, the irradiances could not have been significantly underestimated by beam loss due to misalignment. These arguments for the veracity of the VSTOS measurements are of course not compelling, since a number of transfers and corrections were involved and unidentified systematic errors may exist; however, we have no evidence that the measurements are less accurate than indicated by the error bars, whereas the ASTOS alignment is clearly questionable. We will therefore adopt a weighted mean of the VSTOS measurements and the ASTOS QTs, normalized to the VSTOS values over H27, as our estimates of the true efficiencies on the blue side. This will bring the blue and red QTs, relative to those predicted, into reasonable agreement with the measured

efficiencies, generally at about 75% of the predicted values, such that the error bars of each overlap.

6.2.5.2 Local Features and Anomalies

The measured efficiencies show some local departures from this global trend that merit further discussion. Of the ASTOS measurements, the L65 QTs toward the short wavelength end of its range on both red and blue sides appear to be somewhat lower, with respect to the predicted values, than the other components and the prism, on the blue side (but not the red), also appears relatively inefficient. The L65 discrepancy appears due to differences in the grating orientation in the FOS and for the JHU measurement set-up, since the drawing specifying the grating angles and blaze direction that was available to the JHU personnel was in error.

An explanation for the reduced efficiency of the prism on the blue side (as compared to the red) is somewhat more elusive. The count rates near the response peak in the June and August APC spectra for the prism appear to compare within ~5%, the August rates being the larger (as expected, due to the higher Digicon operating voltage). A more detailed comparison is precluded because the June data (for this exposure only!) were not properly recorded on tape. It is noteworthy, however, that the shape of the spectrum through the upper aperture of the 'A4' pair used deviates considerably from that through lower, with deviations between the two as large as 30%, and that both spectra show multiple small-scale features not seen in the red-side spectra. A possible explanation is that the photo-

cathode suffers some non-uniformity (or a small smudge or particle is present on the detector window) in the very small area over which the prism spectrum extends. This deserves further investigation as the flat fielding data are reduced in the near future. It is important to note that no attempt at flat-fielding the APC spectra has been made; the purpose of this exercise is to determine the overall FOS absolute efficiency on a fairly coarse scale.

For the VSTOS measurements, we first note that in general the agreement among the QTe resulting from spectra of each of the five lamps is well within the errors expected from lamp fluctuation. Notable departures from this trend are the hydrogen lamp results at long wavelengths, which tend to drop below the other measurements increasingly with wavelengths. A large part of this discrepancy is probably due to a real change in the spectral distribution of the hydrogen lamp, although such differences are not evident in the pre- and post-test NBS calibrations of this lamp. However, as indicated in Section 6.2.3.3, this lamp seems to be particularly susceptible to output variations, possibly dependent on its environment and orientation. The Pt-Or-Ne #1 (diffused) lamp measurements also appear a bit lower than the mean of the others, especially for the lines below 11800 in the H19 and L15 spectra. We suspect that this may be due to improper matchings of the NBS and FOS spectral resolution, perhaps combined with some loss of signal in the L15 spectrum, due to nonrepeatability of the FOS filter-grating wheel. The latter may be inferred by noting that the Pt-Or-Ne #1 measurements match

the other lamps quite well in the H19 (above 11800) and prism spectra in the same wavelength region, so their relative calibrations are accurate. The former may be a problem because of the high line density of the Pt spectrum, the poor resolution of the NBS measurements and the use of a rectangular (simple binning of the FOS spectra over the NBS λ) approximation to the true NBS monochromator resolution profile.

The VSTOS QTs, when viewed relative to the predicted values, show two noteworthy features: a sharp, high efficiency peak near 11650, and a broad, shallow dip in the measured efficiency about 2000 Å. These features are not peculiar to a single disperser; the 11650 feature can be seen in H13, H19, and L15 and the 12000 dip in H19, H27, L15, and the prism. Inspection of Figure 6.2.3.3-4 (L15) shows that the former anomaly is due to the lack of the predicted dip in efficiency for the measured QTs. This dip is known, however, to be a typical feature of L_x -optimized MgF_2/Al coatings, such as those used on the FOS collimators, FUV gratings, and the mirror used with the prism. The depth of the feature in the predicted QT curve is not abnormal for two such reflections, although this varies considerably and has been correlated with the degree of surface roughness of the substrate. The absence of this dip is therefore quite unusual, and we can offer no ready explanation.

The 12000 dip is less prominent, and if the 11650 feature were not present, it might be seen rather as a general decrease in efficiency with wavelength below ~ 2600 Å. In either interpretation, the dip may be construed as a manifestation of some

degree of surface contamination. In particular, a broad reduction in efficiency about 12000 is a signature of surface contamination for La -optimized (250 \AA thick) MgF_2 over Al coatings, since the MgF_2 layer is of quarterwave thickness at $\sim 2000 \text{ \AA}$, causing a greater degree of coupling to the surface contaminant at those wavelengths (Heaney et al., 1977, Hass and Hunter 1970). In any case, the implied contamination is not gross; the ratio of the measured to predicted QT is nearly the same in the FUV as in the visible.

6.2.5.3 Final QT Estimates

With the considerations mentioned above in mind, we proceed to make our best estimate of the QT for each FOS configuration. For the blue side VSTOS results, generally the mean of the individual measurements made with each lamp, weighted according to the estimated uncertainty, was taken and a smooth curve drawn through these points. Extrapolation of the data was required below $\sim 1300 \text{ \AA}$ for the H13 and H15 gratings. The single measurement of H13 at 11248 appears exceptionally high (at 86% of the predicted value), so our extrapolation lies about 15% below this value at $\sim 70\%$ of predicted, which is representative of the measurements over most of the spectral range of that grating.

The blue side ASTOS QTs were normalized, as described in Section 6.2.5.1, to bring the H27 measurement into agreement with the VSTOS values. Since the shape of the H27 efficiency curves from each STOS match in the overlap region ($112500\text{-}3000 \text{ \AA}$), only minor smoothing was required to yield a continuous QT curve. However, a 15-20% discrepancy remains between the VSTOS and ASTOS

measurements of the prism, indicating (again) that the latter measurement is peculiar. Nevertheless, since a clear explanation for the low ASTOS result is currently lacking, we have elected to manually smooth the data through the overlap region, adopting the measurements outside that region without further major adjustment. The slope of the QT curve in the 112600-3000 Å interval is likely to be somewhat incorrect as a result. Minor adjustments (not exceeding 2%) have been made to the ASTOS measurements in a few places to smooth the result, since measurement error can produce local variations of this magnitude.

The red side ASTOS measurements have generally been adopted directly, again with minor local smoothing. Since no measurements were made below 2500 Å on the red side, we must estimate the efficiency of L16 and H19 and the blueward portions of the wavelength ranges of the prism and H27 by assuming the predicted values are accurate relative to one another (as argued in Section 6.2.5.1) and scaling the blue side VSTOS results accordingly. This results in some discontinuity in the region of overlap (111500-3000 Å) between the direct ASTOS measurements and the inferred UV values. Although the shapes and slopes are reasonably well matched, the H27 measurements fall ~10% below the inferred values, while the prism measurements are ~15% high. The latter is due partially to the anomalously low blue prism measurement (see above), but in both cases the agreement is well within the errors in the determination of the predicted red QTs relative to those on the blue side and the APC measurement errors. The (more uncertain) inferred values for the short wave-

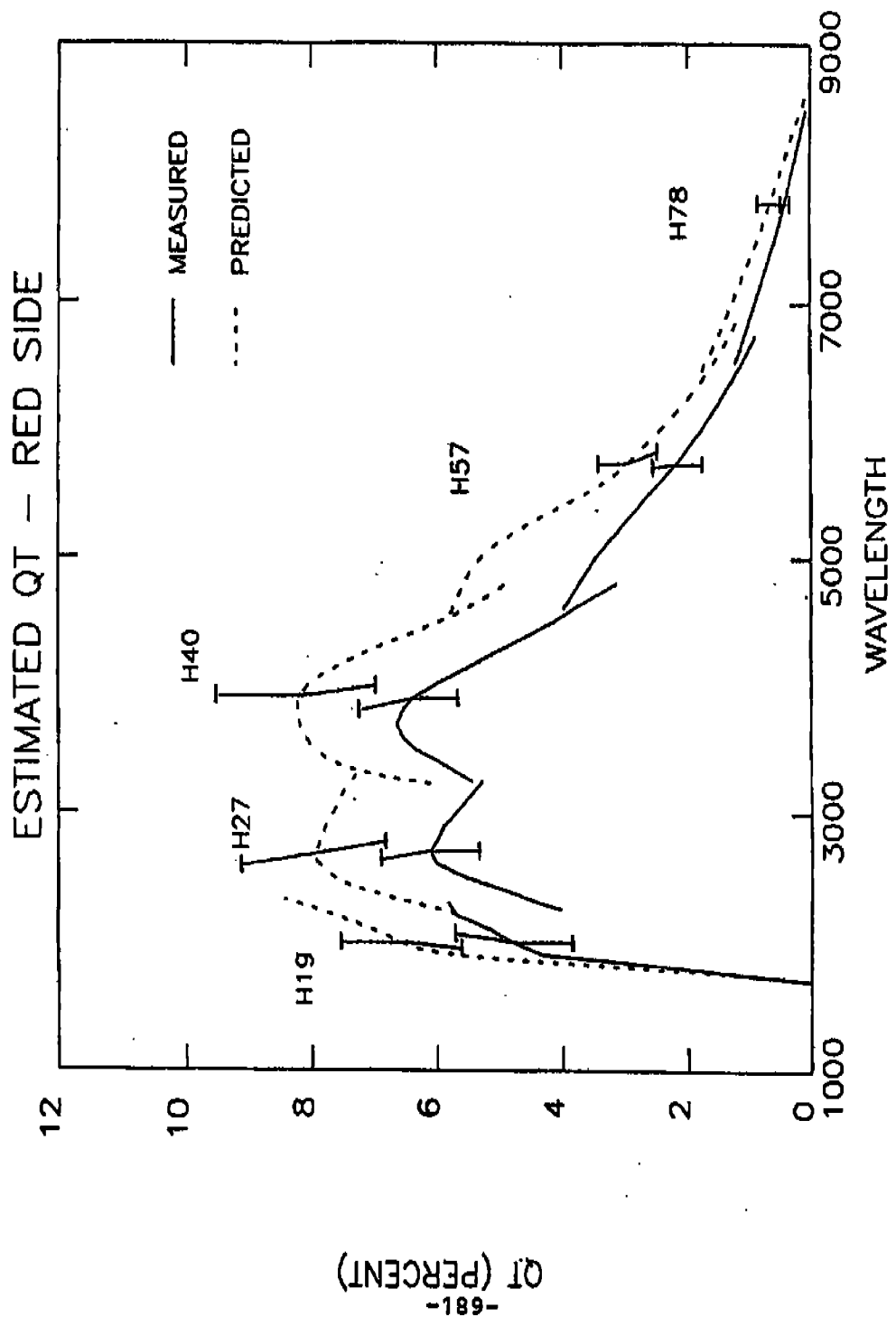


Figure 6.2.5.3-1. Final QT Estimates - Red Side High Resolution Gratings

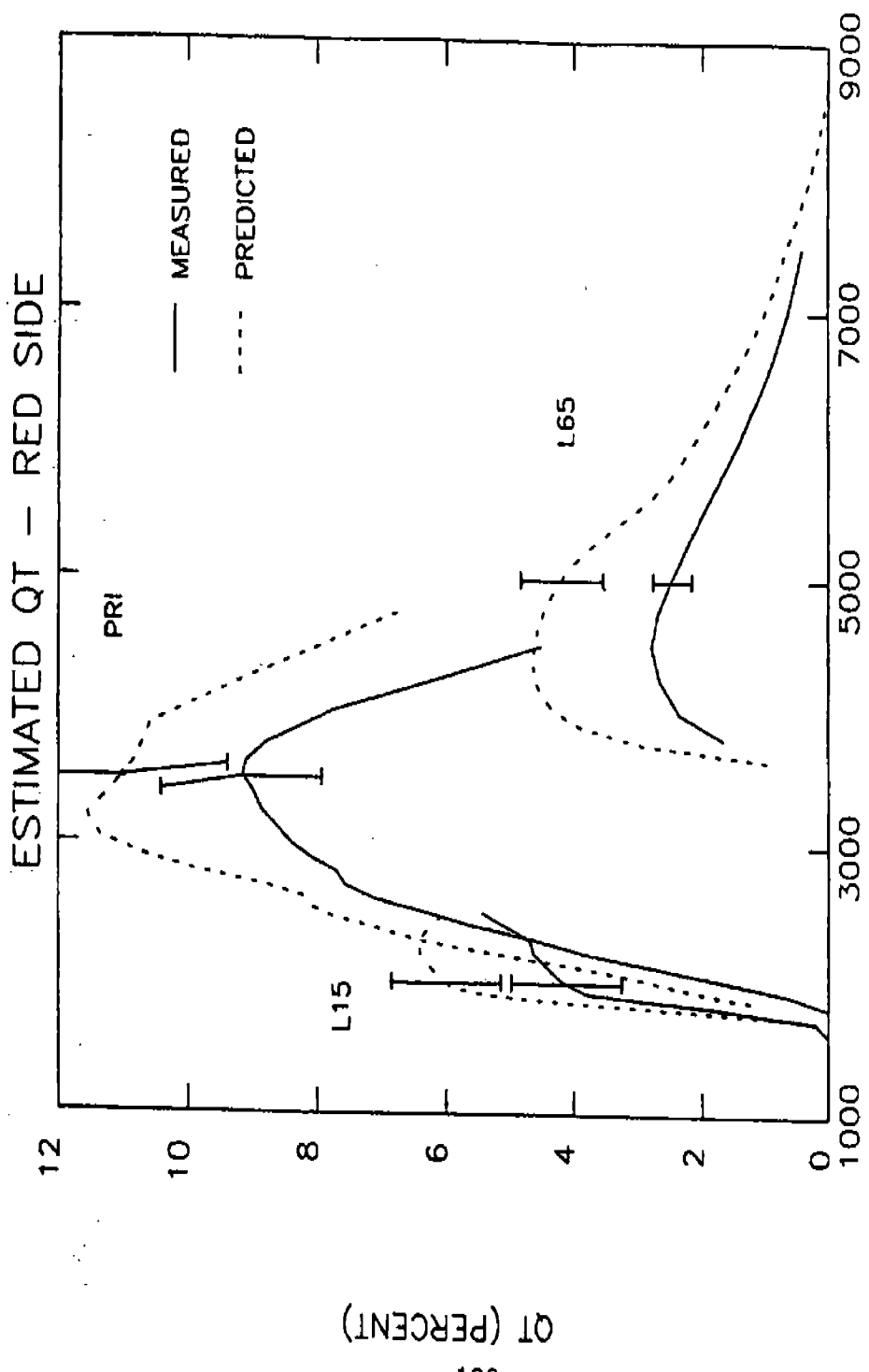


Figure 6.2.5.3-2. Final QT Estimates - Red Side Low Resolution Dispersers

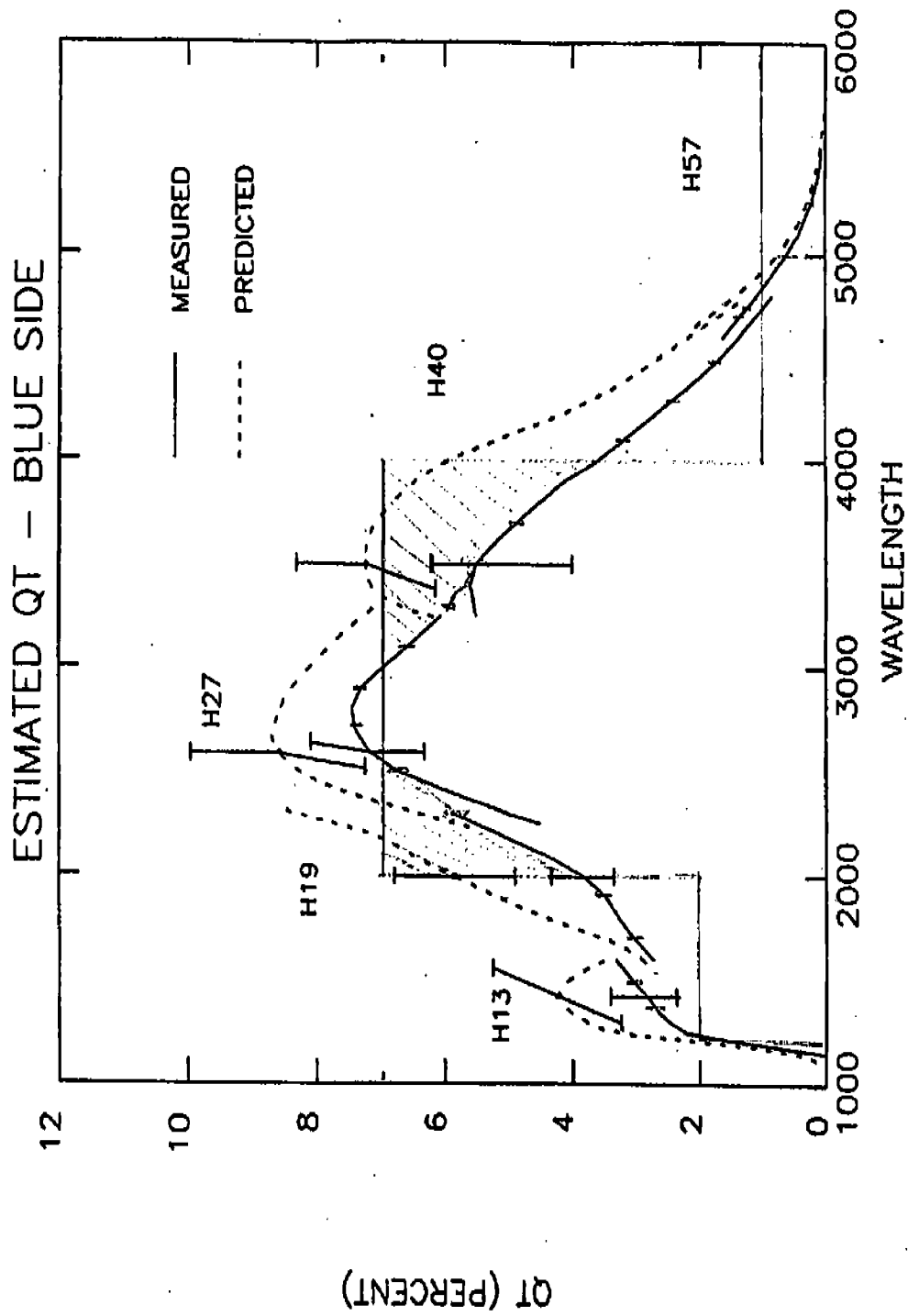


Figure 6.2.5.3-3. Final QT Estimates - Blue Side High Resolution Gratings

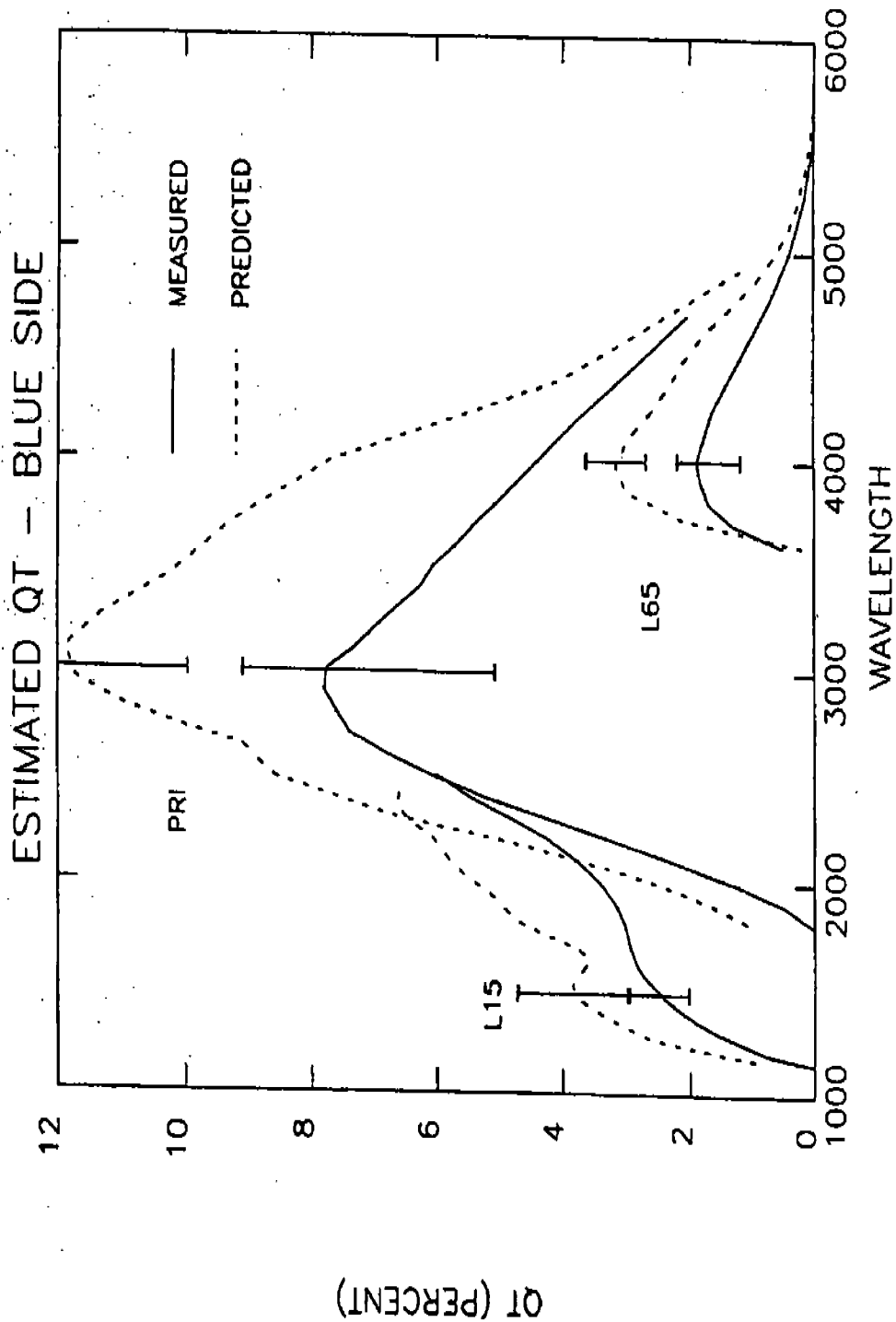


Figure 6.2.5.3-4. Final QT Estimates - Blue Side Low Resolution Dispersers

lengths have been normalized to the measured QTs in order to preserve the shape of the efficiency curve; small residual discrepancies were removed to produce a smooth curve. The final estimated QTs are presented, with the predicted values superimposed as dashed curves, in Figures 6.2.5.3-1 through 6.2.5.3-4. Error bars representing our estimates of the interval in which the true FOS QT must reside are included.

6.2.5.4 Conclusions

The primary conclusion which we may draw from the APC data here presented is that the FOS is in good condition, with high sensitivity over its entire spectral range from the far UV to the near IR. Each of its dispersers and both Digicons demonstrate efficiencies that are a large fraction of those expected on the basis of measurements of the individual components. Furthermore, these predictions and the "end-to-end" APC measurements are generally in agreement within the estimated limits of the measurement errors associated with each.

Nevertheless, our best estimates of the system QTs are in general about 20-25% lower than the predicted values, and little global variation in their ratio is present over the entire wavelength range, on either red or blue side (although the red QTs in the FUV were not directly measured and our estimates were therefore guided by the predicted values). If this degradation is real, we note that it represents an average depreciation in reflectance or transmittance of the four to six exposed optical surfaces used for any particular configuration of 4-6%. This is

not unreasonable, especially since the optics have previously been noted to be less than pristine (e.g., Herzig, 1984).

Some part of the difference between predicted and measured QT may well be due to STOS misalignment, however. Inaccurate alignment of each STOS with the FOS is a major (and difficult to quantify) source of uncertainty in the QT determinations, because of the close match of the output beams to the focal ratio of the FOS. Because the alignment of the STOSs with the NBS calibration facility was either very insensitive (ASTOS) or performed by maximizing the signal (VSTOS), and since their alignment with the FOS was both critical and difficult to perform and check, underestimates of the true FOS QTs are likely to have resulted. The evidence for such misalignment of the ASTOS on the blue side was considered convincing enough to warrant normalizing those data to the VSTOS measurements.

A wavelength-independent reduction in system efficiency can also be the result of some internal misalignment of the FOS optics, such as improper tilt of the collimator such that the beam partially misses the gratings, or a baffle vignetting the beam. An inspection of the blue side optical train just prior to delivery to LMSC, although performed under less than ideal conditions, revealed no obvious obstructions or misalignments that could account for losses as great as 20%, but smaller effects cannot be ruled out on the basis of that inspection.

Future measurements, if the schedule permits any further evaluation of the FOS efficiency, should be performed in such a manner as to reduce the uncertainties due to misalignment. One

such technique is the utilization of two beam focal ratios, one clearly underfilling the FOS optics (e.g., f/30), thereby minimizing sensitivity to both alignment and diffraction by the smaller apertures, and the other filling the optics at f/24. The latter should be used to align the STOS by maximizing the signal; a small effort to provide a reasonable way to articulate the STOS would aid this greatly.

We conclude by reiterating that the FOS has been found "healthy" and free from any major debilitating contamination, and can be expected to perform efficiently in each of its observing configurations.

6.3 Location of Spectra

6.3.1 Introduction

The optimum method of determining the locations and orientations of FOS spectra on the two-dimensional Digicon photocathodes is described. The Y-center of a spectrum as a function of diode number deviates from linearity by up to 15 microns, because of small distortions in the magnetic focusing fields in the Digicons. In addition, the spectra are rotated by small angles (typically 0.005 for the high resolution gratings) with respect to the diode array. This report presents all spectral position and orientation measurements since the replacement of the Digicons in the second quarter of 1984. Average shifts in spectral position are computed between calibrations at different temperatures and at different Digicon voltages.